Dopamine transporter trafficking and Rit2 GTPase:

In vivo impact and mechanism of action

Rita R. Fagan[1], Patrick J. Kearney[1], Carolyn G. Sweeney[1*], Dino Luethi[2], Florianne S. E. Uiterkamp[2#], Klaus Schicker[2], Lauren C. O'Connor[1], Harald H. Sitte[2], and Haley E. Melikian[1]

[1]Brudnick Neuropsychiatric Research Institute, Department of Neurobiology, University of Massachusetts Medical School, Worcester, MA, 01605

[2]Medical University Vienna, Center for Physiology and Pharmacology, Institute of Pharmacology, Vienna, Austria, A-1090

Corresponding author email: haley.melikian@umassmed.edu

Current affiliations: [*]Eaton-Peabody Laboratories, Massachusetts Eye and Ear Infirmary, Harvard Medical School, Boston, MA; [#]Institute of Science and Technology, Klosterneuburg, Austria

ABSTRACT

Following its evoked release, extracellular dopamine (DA) levels are stringently controlled by presynaptic reuptake, mediated by the cocaine-sensitive dopamine (DA) transporter (DAT). Multiple DAT coding variants have been identified in DA-related neuropsychiatric disorders, illustrating DAT's integral role in maintaining DAergic homeostasis. DAT is dynamically regulated by endocytic trafficking. Protein kinase C (PKC) activation accelerates DAT internalization and acutely diminishes DAT surface expression. In cell lines, PKC-stimulated DAT endocytosis requires both Ack1 inactivation, which releases a DAT-specific endocytic brake, and the neuronal GTPase, Rit2, which binds DAT. However, it is unknown whether PKC-stimulated DAT endocytosis in DAergic terminals requires Rit2, or whether there are region- or sex-dependent differences in Rit2-dependent DAT trafficking. Moreover, the intrinsic determinants that mediate the DAT-Rit2 interaction are undefined, as are the mechanisms through which Rit2 controls PKC-stimulated DAT endocytosis. Here, we leveraged an AAV-mediated approach to conditionally knockdown Rit2 *in vivo* in DAergic neurons, and found that Rit2 was required for steady state DAT surface expression and PKC-stimulated DAT internalization, with marked sex- and region-specific differences. FRET and surface pulldown studies in cell lines revealed that PKC activation drives DAT-Rit2 surface dissociation, and the DAT N-terminus is required for both DAT-Rit2 dissociation and stimulated DAT internalization in response to PKC activation. Finally, we found that Rit2 and Ack1 independently converge on DAT to facilitate PKC-stimulated DAT endocytosis. Together, our data provide greater insight into mechanisms that mediate PKC-regulated DAT internalization, and reveal striking

region- and sex-specific differences in PKC-stimulated DAT trafficking in *bona fide* DAergic terminals.

INTRODUCTION

Dopamine (DA) neurotransmission is required for motor control, learning, memory, motivation, and reward (Wise 2004; Iversen and Iversen 2007). DAergic dysregulation is evidenced in numerous neuropsychiatric disorders, including attention-deficit/hyperactivity disorder (ADHD), autism spectrum disorder (ASD), schizophrenia, bipolar disorder, addiction, and Parkinson's disease (PD) (Hyman, Malenka, and Nestler 2006; Sharma and Couture 2014; Ashok et al. 2017; Howes et al. 2017; Eissa et al. 2018; Geibl, Henrich, and Oertel 2019). DA signaling is tightly controlled by the presynaptic dopamine transporter (DAT), which rapidly clears synaptically released DA. DAT is also the primary target for addictive and therapeutic psychostimulants, including amphetamine (AMPH), cocaine, and methylphenidate (Ritalin), which inhibit DAT as competitive substrates (AMPH) and antagonists (cocaine and methylphenidate) (Kristensen et al. 2011). Genetic DAT deletions in mice and *Drosophila melanogaster* elevate extracellular DA concentrations and evoke hyperactivity (Gainetdinov et al. 1998; Giros et al. 1996; Kume et al. 2005), and human DAT missense mutations have been reported in PD, ADHD and ASD patients (Mazei-Robison and Blakely 2005; Kurian et al. 2009; Sakrikar et al. 2012; Hamilton et al. 2013; Ng et al. 2014; Bowton et al. 2014; Herborg et al. 2018). Together, these studies underscore that DAT is critical to maintain DAergic homeostasis (Kristensen et al. 2011).

Given its central role in DAergic signaling, intrinsic neuronal mechanisms that alter DAT surface expression and function are likely to significantly impact DAergic transmission. DAT surface availability is dynamically regulated by endocytic recycling (Melikian 2004; Eriksen et al. 2010; Bermingham and Blakely 2016). A negative regulatory mechanism, or “endocytic brake”, tempers basal DAT endocytosis (Boudanova et al. 2008; Wu et al. 2015), and acute protein kinase C (PKC) activation disengages the DAT endocytic brake, stimulates DAT internalization, and rapidly diminishes DAT surface expression (Loder and Melikian 2003; Gabriel et al. 2013). The DAT amino- and carboxy-termini encode residues required to engage the DAT endocytic brake, and, when mutated, markedly accelerate DAT internalization (Boudanova et al. 2008; Sorkina et al. 2009; Sakrikar et al. 2012). We previously reported that non-receptor tyrosine kinase, Ack1 (TNK2), is a critical component of the DAT endocytic brake, and that Ack1 inactivation is required for PKC-mediated brake release (Wu et al. 2015).

Rit2 (AKA: Rin) is a neuron-specific, small GTPase that lacks a CAAX domain, and associates with the plasma membrane in a phosphoinositide-dependent manner (Lee et al. 1996; Wes, Yu, and Montell 1996; Heo et al. 2006). Rit2 activity is required for NGF-mediated p38 MAP kinase and ERK activation in neuroendocrine cells (Shi, Han, and Andres 2005; Uenaka et al. 2018). Moreover, Rit2 gene expression is enriched specifically in DA neurons (Zhou et al. 2011), and several recent GWAS studies identified Rit2 SNPs and long tandem repeat variants associated with multiple DA-related disorders, including Parkinson’s disease, ASD, and schizophrenia (Glessner et al. 2010; Pankratz et al. 2012; Zhang et al. 2015; Emamalizadeh et al. 2017; Foo et al. 2017; Hamedani et al. 2017). However, despite its disease association, relatively little is

known about endogenous DAergic Rit2 function. We previously reported that DAT directly binds to Rit2, and that Rit2 activity is required for PKC-stimulated DAT internalization (Navaroli et al. 2011). Moreover, we recently found that *in vivo* DAergic Rit2 knockdown (Rit2-KD) differentially alters acute cocaine sensitivity in males and females (Sweeney et al. 2019). However, it remains unknown whether PKC-stimulated DAT internalization in DAergic terminals requires Rit2, and whether there are region- or sex-specific differences in DAT's reliance upon Rit2. Further, it is unclear which intrinsic DAT determinants are required for the DAT-Rit2 interaction, or whether Rit2 and Ack1 coordinate to release the DAT endocytic brake. In the present study, we took advantage of a variety of biochemical and genetic approaches in both cultured cells and *ex vivo* mouse striatal slices to directly address these salient questions.

MATERIALS AND METHODS

Materials: Phorbol 12-myristate 13-acetate (PMA) was from LC Laboratories (P-1680) and AIM-100 was from Tocris-Cookson. All other reagents were from either Sigma-Aldrich or Fisher Scientific, and were of the highest possible grade.

Animals: All studies were conducted in accordance with UMASS Medical School IACUC Protocol A-1506 (H.E.M). *Pitx3*$^{IRES2\text{-}tTA}$ mice on the *C57Bl/6* background were the generous gift of Dr. Huaibin Cai (National Institute on Aging), and were continually backcrossed to *C57Bl/6* mice. Mice were maintained in 12hr light/dark cycle at constant temperature and humidity and food and water were available ad libitum.

Antibodies: Primary antibodies used: mouse anti-Rit2 18G4 (27G2; Sigma), mouse anti-Rit2 OTI4B5 (Origene Technologies Inc.), rat anti-DAT (MAB369), mouse anti-SERT (ST51-2; Mab Technologies), rabbit anti-HA (C29F4; Cell Signaling Technology), mouse anti-GFP (Roche), mouse anti-Ack1 (A-11; sc-28336), and rabbit anti-pY284-Ack1 (Millipore). Horseradish peroxidase-conjugated secondary antibodies: goat anti-rat, goat anti-mouse and goat anti-rabbit were from Jackson ImmunoResearch.

Plasmids and cloning: N-S/DAT (SERT1-78/DAT60-620), DAT/C-S (DAT1-583/SERT601-630), and S/DAT/S (SERT1-78/DAT60-583/SERT601-630) plasmids, in which either the DAT N-terminus (N-S/DAT), C-terminus (DAT/C-S), or both termini (S/DAT/S) were substituted with those of SERT, were generated as previously described (Sweeney et al. 2017) using PCR-ligation-PCR approach to clone the DAT or

SERT terminal domains onto the hSERT or hDAT-pCDNA3.1(+) backbone. CFP-tagged chimeras were generated by cloning their cDNAs into the pECFP-C1 vector using HindIII/XbaI (N-S/DAT), HindIII (DAT/C-S), and HindIII/SalI (S/DAT/S). Bungarotoxin binding site (BBS)-tagged hDAT and DAT chimera constructs were generated using the extracellular tagging strategy as previously described (Wu et al. 2017) with the following amino acid sequence inserted into extracellular loop 2 of hDAT and DAT chimera constructs: GSSGSSGWRYYESSLEPYPDGSSGSSG. The underlined BBS is flanked by linker sequences. All plasmids were verified by Sanger sequencing (Genewiz). Human constitutively active Ack1 mutant (S445P-Ack1-HA) was generated as previously described (Wu et al. 2015).

AAV production and stereotaxic viral delivery: pscAAV-TRE-eGFP and pscAAV-TREmiR33-shRit2-eGFP plasmids were generated as previously described (Sweeney et al. 2019), and AAV particles (AAV9 serotype) were produced, purified, and titers determined by the University of Massachusetts Medical School Viral Vector Core, as previously described (Mueller et al. 2012). For intracranial stereotaxic AAV injections, male and female mice (minimum 3 weeks age) were anesthetized with 100mg/kg ketamine/10mg/kg xylazine (I.P.), and 20% mannitol was administered (I.P.) 15 minutes prior to viral delivery, to increase viral spread (Burger et al. 2005). Mouse heads were shaved, placed in the stereotaxic frame, and bilateral 0.8mm holes were drilled into the skull at the indicated stereotaxic coordinates. 1µl of the indicated viruses were infused bilaterally into the VTA (Bregma: anterior/posterior: -3.08mm, medial/lateral: ±0.5mm, dorsal/ventral: -4.5mm) at a rate of 0.2µL/min. Syringes were left in place for a minimum

of 5 minutes post-infusion prior to removal. Mice were housed for a minimum of four weeks before experiments were performed. Viral expression in each animal was confirmed by visualizing GFP expression in 0.3mm coronal ventral midbrain slices.

Ex vivo slice biotinylation: Ex vivo striatal slices were prepared 3-4 weeks following viral injection. Mice were sacrificed by cervical dislocation and rapid decapitation and heads were immediately submerged in ice cold, oxygenated cutting solution, pH 7.4 (in mM: 20 HEPES, 2.5 KCl, 1.25, NaH_2PO_4, 30 $NaHCO_3$, 25 glucose, 0.5 $CaCl_2 \cdot 4H_2O$, 10 $MgSO_4 \cdot 7H_2O$, 92 N-methyl-D-glucamine (NMDG), 2.0 thiourea, 5.0 Na^+-ascorbate, 3.0 Na^+-pyruvate) for 1 min. Brains were removed and 300µm coronal slices were prepared with a VT1200 Vibroslicer (Leica) in ice-cold, oxygenated cutting solution. Slices were hemisected along the midline, and were recovered in ACSF, pH 7.4 (in mM: 125 NaCl, 2.5 KCl, 1.24, NaH_2PO_4, 26 $NaHCO_3$, 11 glucose, 2.4 $CaCl_2 \cdot 4H_2O$, and 1.2 $MgCl_2 \cdot 6H_2O$) 40 min, 31°C. Hemi-slices were treated ±1µM PMA in ACSF, 30min, 37°C with constant oxygenation, using their contralateral hemi-slice as a vehicle-treated control. Following drug treatment, slices were moved to ice and surface DAT was labeled by biotinylation as previously described (Gabriel et al. 2013; Wu et al. 2015; Sweeney et al. 2019). Briefly, slices were biotinylated with membrane-impermeant sulfo-NHS-SS-biotin (1mg/ml), 45min, 4°C. Residual biotin was quenched 2x 20 min washes of ice-cold ACSF supplemented with 100mM glycine, and were washed with ice-cold ACSF. Hemi-slices were enriched for dorsal and ventral striatum, by sub-dissecting in a line from the anterior commissure to the lateral olfactory tract. Sub-dissected slices were lysed in RIPA buffer containing protease inhibitors, and tissue

was disrupted by triturating sequentially through a 200µL pipet tip, 22G and 26G tech-tips. Samples rotated 30min at 4°C to complete lysis, insoluble material was removed by centrifugation, and protein concentrations were determined using the BCA protein assay. Biotinylated proteins were isolated by batch streptavidin chromatography, overnight with rotation, 4°C, at a ratio of 20µg striatal lysate to 30µL streptavidin agarose beads, which was empirically determined to recover all biotinylated DAT. Recovered proteins were washed with RIPA buffer and eluted from beads in 2X SDS-PAGE sample buffer, 30min, room temperature with rotation. Eluted (surface) proteins and their respective lysate inputs were resolved by SDS-PAGE, and DAT was detected by immunoblotting as described above. %DAT at the cell surface was determined by normalizing surface signals to the corresponding total DAT input signal in a given hemi-slice, detected in parallel, and were further normalized to vehicle-treated contralateral hemi-slice controls. Note that DAT surface levels from male, vehicle-treated hemislices were previously reported by our laboratory (Sweeney et al. 2019). These values were used to determine the %change in DAT surface levels following PMA treatment of their respective, contralateral hemislices, which we report in this study.

Cell Culture and transfection: Cells were maintained at 37°C, 5% CO2. SK-N-MC cells were grown in MEM (Sigma), and HEK293T, HEK293 (FRET studies) and N2a cells were grown in DMEM (CellGro/Corning), each supplemented with 10% fetal bovine serum, 2mM glutamine, and 100 units/mL penicillin-streptomycin. SK-N-DZ cells were grown in DMEM (ATCC #30-2002) supplemented with 10%FBS, 1X non-essential amino acids (Gibco) and 100u/mL penicillin-streptomycin. HEK293T cells were

transfected using Lipofectamine 2000 (Invitrogen) according to manufacturer's instructions with the following modifications: For biochemical and RT-qPCR studies, cells were seeded into 6-well plates at a density of $1x10^6$ (SK-N-MC), $5x10^5$ (HEK293T), or $2.5x10^5$ (N2a) cells/well one day prior to transfection, and were transfected with 3µg (SK-N-MC) or 2µg (HEK293T and N2a) plasmid DNA/well using a lipid:DNA ratio of 2:1 (SK-N-MC and HEK293T) or 4:1 (N2a). Stable cell lines were generated by selecting cells starting 48 hrs following transfection, with 0.5 mg/mL (SK-N-MC) or 0.8 mg/L (SK-N-DZ) G418 (Geneticin, Invitrogen/Life Technologies). Stably transfected cells were pooled and cell lines were maintained under selective pressure using 0.2 mg/mL or 0.32 mg/mL G418 for SK-N-MC and SK-N-DZ cells, respectively. For FRET imaging studies, HEK293 cells were seeded into an 8-well chambered coverslip (ibidi) at a density of $2x10^4$ cells/well one day prior to transfection, and were transfected with the indicated plasmids using JetPRIME (Polyplus-transfection) according to the manufacturer's protocol. FRET studies were performed 24 hrs post-transfection.

shRNA, Lentiviral production and cell transduction: GIPZ lentiviral shRNA constructs targeted to Rit2, and empty pGIPZ vector control, were obtained from Dharmacon. Tested shRNA clone ID's and mature antisense sequences were as follows:

shRit2-104: V3LHS_380104; CTTCTTCTTCAAAGAACCT
shRit2-105: V3LHS_380105; TTGTTACCCACCAGCACCA
shRit2-107: V3LHS_380107; CTTCTTCTTCAAAGAACCT

Lentiviral particles were produced in HEK293T cells as previously described (Wu et al. 2015). For cell transduction, $1x10^6$ cells stable DAT-SK-N-DZ cells were seeded onto 6-well plates one day prior to viral transduction. 3.0mL of lentiviral supernatant,

supplemented with 0.8µg/mL polybrene, was added. 24 hrs post-infection, transduced cells were selected for an additional 72 hrs by replacing media with SK-N-DZ media supplemented with 1.25µg/mL puromycin. Assays were conducted 96 hrs post-transduction.

FRET: FRET was measured using an iMIC inverted microscope (TILL Photonics GmbH). Samples were focused using a 60X (N.A. 1.49) oil objective (Olympus). Fluorescence was excited using a 100 W Xenon Lamp (Polychrome, Till Photonics GmbH). Excitation light was filtered through either a 436/20 nm (CFP) or 514/10 nm (YFP) excitation filter (Semrock) and directed to the sample via a 442/514 dual line dichroic mirror (Semrock). Emitted fluorescence light was filtered through a 480/40 nm - 570/80 nm dual emission filter (Semrock) and directed to a beamsplitter unit (Dichrotom, Till Photonics). Briefly the emission light was separated spatially according to the fluorescence wavelength using a 515 nm dichroic mirror (Semrock). The resultant two channels (<515 nm & >515 nm) were projected next to each other onto an EMCCD chip (iXon Ultra 897Andor) and recorded using Live Acquisition software (version 2.5.0.21; TILL Photonics GmbH). To guarantee the best signal to noise ratio and dynamic range, the camera was operated in 16-bit mode with a readout speed of 1 MHz. According to manufactories recommendation; an EM-Gain of 16 was applied to overcome the noise floor. To analyze FRET (see below) two images were taken per set (Donor excitation -> Donor Emission / Acceptor Emission and Acceptor Excitation -> Acceptor Emission respectively). Per condition ten sets were recorded each experimental day; the images were then analyzed using Offline Analysis software (version 2.5.0.2; TILL Photonics

GmbH). One region of interest (part of the plasma membrane) per cell was selected in the CFP channel. Background fluorescence was subtracted from each image and the average intensity of each region of interest was used for calculations. Spectral bleed through (BT) for donor (0.57) and acceptor (0.04) was determined using HEK293 cells expressing a CFP or YFP signal only. Normalized FRET (NFRET) was calculated as follows:

$$\mathrm{NFRET} = \frac{I_{FRET} - (BT_{Donor} \times I_{Donor}) - (BT_{Acceptor} \times I_{Acceptor})}{\sqrt{I_{Donor} \times I_{Acceptor}}}\ x\ 100$$

A fused CFP-YFP construct (CYFP) was included as positive control, resulting in maximum FRET. Non-fused donor and acceptor fluorophores were included as a negative control.

RNA extraction & RT-qPCR: RNA was isolated from cell lines using RNAqueous®-Micro Kit RNA Isolation (Thermo Fisher Scientific). Reverse transcription was performed using RETROscript® Reverse Transcription Kit (Thermo Fisher Scientific). Quantitative PCR was performed and analyzed using the Applied Biosystems® 7500 Real-Time PCR System Machine and Software, using Taqman® Gene Expression Assays for Human Rit2 (Hs_01046673_m1) and human GAPDH (Hs_99999905_m1).

[^{3}H]DA uptake assay: SK-N-MC cells stably expressing BBS-DAT were seeded onto 96-well plates at a density of 7.5x10^4/well 24 hrs prior to assay. Cells were washed twice with Krebs-Ringer-HEPES buffer (120mM NaCl, 4.7mM KCl, 2.2mM $CaCl_2$, 1.2mM $MgSO_4$, 1.2mM KH_2PO_4, and 10mM HEPES, pH 7.4) and pre-incubated in KRH

supplemented with 0.18% glucose ±1μM PMA, 30 min, 37°C. 100nM desipramine was included in all samples to eliminate uptake contribution of endogenous norepinephrine transporter. DA uptake was initiated by addition of 1μM [^{3}H]DA (Perkin Elmer: Dihydroxyphenylethylamine (Dopamine), 3,4-[Ring-2,5,6-^{3}H]) in KRH supplemented with 0.18% glucose, 10μM pargyline, and 10μM ascorbic acid. Assays proceeded for 10min, 37°C, and were terminated by three rapid washes with ice-cold KRH buffer. Cells were solubilized in scintillation fluid, and accumulated radioactivity was determined by liquid scintillation counting in a Wallac MicroBeta scintillation plate counter. Non-specific DA uptake was defined in the presence of 10μM GBR12909.

Internalization Assays and Immunoblotting: Relative internalization rates over 10 minutes were measured by reversible biotinylation as previously described (Loder and Melikian 2003; Wu et al. 2017). Briefly, the indicated stably transfected cells were seeded into 6-well plates at 1.5x10^6 cells/well one day prior to analysis. Cells incubated twice with 2.5 mg/mL sulfo-NHS-SS-biotin (15 min, 4°C) and quenched twice with PBS^{2+} (PBS, pH 7.4, 1.0mM $MgCl_2$, 0.1mM $CaCl_2$) supplemented with 100mM glycine (15 min, 4°C). Internalization was initiated by rapidly warming cells in prewarmed PBS^{2+} supplemented with 0.18% glucose, 0.2% protease-/IgG-free bovine serum albumin, and proceeded for 10min, 37°C in the presence of the indicated drugs. Parallel surface-labeled controls remained at 4°C. Cells were rapidly cooled by washing thrice with ice-cold NT buffer (150mM NaCl, 20mM Tris, pH 8.6, 1.0mM EDTA, pH 8.0, 0.2% protease-/IgG-free bovine serum albumin) and remaining surface biotin was stripped by reducing in 100mM TCEP in NT buffer twice (25 min, 4°C). Cells were rinsed rapidly in PBS^{2+},

and were lysed in RIPA buffer (10mM Tris, pH 7.4, 150mM NaCl, 1.0mM EDTA, 0.1% SDS, 1% Triton-X-100, 1% sodium deoxycholate) containing protease inhibitors (1.0mM PMSF and 1.0g/mL each leupeptin, aprotinin, and pepstatin). Lysates were cleared by centrifugation and protein concentrations were determined with the BCA protein assay (Thermo Fisher) using BSA as a standard. Biotinylated proteins were recovered by streptavidin batch chromatography from equivalent amounts of cell lysate, and were eluted in 2X Laemmli sample buffer, 30 min, room temperature with rotation. Eluted proteins were resolved by SDS-PAGE and proteins were detected and quantified by immunoblotting: hDAT and DAT/C-S were detected with amino-directed rat anti-DAT (MAB369, Millipore, 1:2000), and N-S/DAT and S/DAT/S were detected with amino-directed mouse anti-hSERT (MAb Technologies,1:2000). Immunoreactive bands were detected using a VersaDoc imaging station (Bio-rad), and were in the linear range of detection. Internalization rates were calculated as %surface protein internalized/10 min, as compared to their respective surface signal at t=0 min (controls that were biotinylated and kept at 4°C). Note that for all representative immunoblots shown throughout the study, all brightness/contrast manipulations were made uniformly across any given blot. For presentation purposes, immunoreactive bands were cropped from the same exposure of the same immunoblot.

BBS-DAT/chimera pulldowns: HEK293T cells were transiently co-transfected with HA-Rit2, and either BBS-DAT or BBS-DAT chimeras, at a DAT:Rit2 plasmid ratio of 1:4, as described above. Cells were washed thrice with ice cold PBS^{2+} and surface BBS-DAT chimeras were labeled with 120μM biotinylated α-bungarotoxin (α-BTX-b, Thermo

Fisher) in PBS^{2+}, 2 hrs, 4ºC. For drug treatments, cells were treated with the indicated drugs 30 min, 37°C, prior to labeling with α-BTX-b. Following labeling, α-BTX-b solution was removed, cells were washed thrice with ice cold PBS^{2+}, and were lysed in ice-cold co-immunoprecipitation (co-IP) lysis buffer (50mM Tris, pH 7.4, 100mM NaCl, 1% Triton X-100, 10% glycerol, and 1.0mM EDTA) containing protease inhibitors (1.0mM PMSF and 1.0g/mL each leupeptin, aprotinin, and pepstatin) and Phosphatase Inhibitor Cocktail V (EMD Millipore), 30 min, 4°C. Labeled proteins were recovered from equivalent amounts of protein by batch affinity chromatography with streptavidin-coupled M280 Dynabeads (Thermo Fisher), 4°C, overnight with rotation. Lysate/bead ratios were empirically determined to assure quantitative recovery of all labeled proteins in lysates. Beads were gently washed thrice with ice-cold co-IP buffer, with magnetic recovery between washes, and isolated proteins were eluted from beads in an equal volume of co-IP lysis buffer and 2X SDS-PAGE sample buffer (100mM Tris, pH 6.8, 4.4% SDS, glycerol, 100mM DTT, and 0.04% bromophenol-blue). Isolated proteins were resolved by SDS-PAGE, and immunoblotted with antibodies for rat anti-DAT (1:2000), mouse anti-hSERT (1:2000), and rabbit anti-HA (1:2000) as indicated above. Immunoreactive HA-Rit2 band densities were normalized to their respective recovered DAT, or chimera, bands in each independent experiment.

Statistical Analysis: All data were analyzed using GraphPad Prism software. Statistical outliers within data sets were determined prior to analysis using either Grubb's or Rout's outlier test, and were removed from further analysis. Specific statistical tests used are

detailed within each figure legend. For comparisons between two groups, a Student's t test was used. For comparison among more than two experimental groups, one-way ANOVA with appropriate post-hoc analyses were performed, as described.

RESULTS

Rit2 cellular expression and antibody specificity

In our previous study (Navaroli et al. 2011), there were several paradoxical findings regarding 1) how PKC activation impacted the DAT-Rit2 interaction, and 2) the Rit2 expression pattern across cell lines. In cellular imaging studies, which used CFP-Rit2, Rit2 appeared to remain at the plasma membrane following PKC-stimulated DAT internalization, suggesting that PKC may drive DAT and Rit2 to dissociate. In contrast, PKC activation increased the DAT-Rit2 interaction in PC12 cells, as detected by co-IP. Furthermore, although Rit2 expression is reportedly restricted to neurons (Lee et al. 1996; Wes, Yu, and Montell 1996; Zhou et al. 2011; Zhang et al. 2013), we detected a single, ~20kDa Rit2-immunoreactive band by immunoblot in all neuronal and non-neuronal cell lines tested, and we further detected Rit2 mRNA expression in these cell lines by standard RT-PCR. The previous studies utilized the anti-Rit2 monoclonal antibody, clone 27G2, and we additionally confirmed that 27G2 specifically recognizes Rit2, but not Rit1, (the ubiquitously expressed Rit2 homologue) using fluorescently-tagged proteins. Recently, we decided to take advantage of highly-specific, Rit2-directed, real-time qPCR probes to re-assess potential Rit2 expression across a large panel of human, mouse and rat cell lines, as well as in mouse and rat midbrain, all of which exhibit the single, 20kDa immunoreactive band when probed with the anti-Rit2 27G2. To our surprise, Rit2 mRNA was undetectable in any of the mouse or rat cell lines tested, whereas a robust Rit2 mRNA signal was detected in both mouse and rat midbrain controls (Table 1). Moreover, among the human cell lines tested, Rit2 mRNA was only detected in SK-N-DZ cells, as previously reported (Zhang et al. 2013) and at

low levels in SH-SY5Y cells. However, SK-N-MC and HEK293T cells expressed markedly less/negligible Rit2 signal than SK-N-DZ cells, ranging from 20-300 fold less (Table I). These results raised the possibility that although 27G2 does recognize Rit2, it also may cross-react with a ubiquitously expressed protein that has an electrophoretic mobility similar to Rit2. To test this, we screened several newer, commercially available anti-Rit2 antibodies using cell lysates from HEK293T cells transfected with HA-Rit2. Consistent with our previous report, clone 27G2 identified a single 20kDa band in both transfected and non-transfected cells (Fig. 1A). However, when immunoblots were probed with anti-Rit2 clone 4B5, an immunoreactive band was only detected in lysates from transfected cells, but not from non-transfected cells, consistent with our RT-qPCR results. Moreover, clone 4B5 detected a ~26kDa immunoreactive band in HA-Rit2-transfected cells, which was identical in mobility to immunoblots probed with anti-HA, in parallel (Fig. 1B). Anti-Rit2 4B5 also detected bands at ~24kDa in mouse striatum and midbrain lysates (Fig. 1B). These immunoblot results were consistent with our qPCR results, and confirmed that most cell lines either do not express Rit2, or express Rit2 at negligible levels. They further support that the 27G2 antibody cannot reliably distinguish between Rit2 and a robust, artifactual, background band. It should also be noted that while 4B5 specifically detects Rit2, it does so with extremely low sensitivity, even when Rit2 is highly overexpressed. Indeed, using the 4B5 antibody, we could only detect Rit2 by immunoblot in lysates from transfected cells or mouse tissues when a very high protein mass was loaded (100μg/lane). Therefore, for the majority of the remaining studies, we opted to use HA-Rit2 for greater sensitivity.

Rit2 is required for PKC-stimulated, but not basal, DAT internalization.

In our previous study, we used shRNA-mediated Rit2 silencing in SK-N-MC cells to test whether Rit2 is required for PKC-stimulated DAT downregulation. In light of our current findings that SK-N-MC cells do not appreciably express Rit2, we were prompted to 1) re-screen Rit2 targeted shRNAs, and 2) reassess whether Rit2 is required for PKC-stimulated DAT internalization in cells that endogenously express Rit2. We screened several putative Rit2-directed shRNAs and identified a human Rit2-directed shRNA (shRit2-107) that significantly silenced both overexpressed GFP-hRit2 protein (Fig. 2A), as well as endogenous Rit2 mRNA expression in SK-N-DZ cells (Fig. 2B). We next utilized shRit2-107 to test whether Rit2 is required for either basal or PKC-stimulated DAT internalization in SK-N-DZ cells. Rit2-KD had no significant effect on basal DAT internalization as compared to vector-transduced controls ($p=0.24$, Student's t test, $n=11$). However, Rit2-KD significantly blocked PKC-stimulated DAT endocytosis (Fig. 2C), consistent with a requisite role for Rit2 in PKC-stimulated DAT internalization.

Rit2 is required for PKC-stimulated DAT downregulation in a region- and sex-specific manner in mouse striatum

Although Rit2 is required for PKC-stimulated DAT internalization in heterologous expression systems, the impact of Rit2 on PKC-stimulated DAT endocytosis in *bona fide* DAergic terminals is unknown. Further, it is unknown whether PKC-stimulated DAT internalization differs between DAergic terminal regions, or between males and females. We recently leveraged the TET-OFF system to achieve AAV-mediated, conditional, inducible DAergic Rit2-KD in *Pitx3*$^{IRES2\text{-}tTA}$ mice, and found that DAergic Rit2 silencing decreased total striatal DAT protein in males, but not females (Sweeney et al. 2019). Further, although total DAT protein decreased within the total striatum in males, the

DAT surface: intracellular ratio was unchanged in either dorsal striatum (DS) or ventral striatum (VS), resulting in less overall surface DAT in both regions (Sweeney et al. 2019). For the current study, we next asked whether Rit2 impacts DAT basal distribution in female DS and VS, and whether PKC-mediated DAT internalization requires Rit2 in male and female DS and VS. Male and female *Pitx3*$^{IRES2\text{-}tTA/+}$ mice VTA were bilaterally injected with either AAV9-TRE-eGFP or AAV9-TRE-shRit2, and DAT surface expression was measured by *ex vivo* slice biotinylation in the VS and DS, following treatment ±1μM PMA, 30 min, 37°C. We first examined the effect of Rit2 silencing on basal DAT surface expression in female mice, determined in vehicle-treated slices. Although Rit2-KD had no effect on total striatal DAT levels in females (Sweeney et al. 2019), it significantly reduced the basal DAT surface: intracellular distribution in the VS (eGFP: 88.3 ±3.7 vs. shRit2: 51.2 ±11.7 %total DAT on surface, p=0.01, two-tailed Student's t test, n=5-6), which, similar to males, translated to a decrease in absolute surface DAT in female VS. In contrast, Rit2-KD had no effect on the DAT surface: intracellular distribution in female DS (eGFP: 37.8 ±5.3 vs. shRit2: 50.2 ±10.3 %total DAT on surface, p=0.27, two-tailed Student's t test, n=5-7). We next asked whether PKC activation drives DAT internalization equivalently in male and female VS and DS and, if so, whether PKC-stimulated DAT internalization requires Rit2. In males, PKC activation significantly decreased DAT surface expression in VS, and Rit2-KD abolished PKC-stimulated DAT internalization as compared to vehicle-treated slices (Fig. 3A). In female mice, PKC activation similarly decreased DAT surface expression in the VS, and Rit2-KD significantly blocked PKC-stimulated DAT internalization (Fig. 3B). Interestingly, in DS, PKC activation did not drive DAT surface loss in either control- or shRit2-injected

male or female mice. Further, in males, following Rit2-KD, PKC activation significantly increased DAT surface expression in DS (Fig. 3C), whereas in females Rit2-KD had no effect on the response to PKC activation in DS (Fig. 3D; p=0.68). Taken together, these data suggest that, in the VS, Rit2 is required to maintain 1) steady state DAT surface levels in females, 2) total DAT protein levels in males, and 3) PKC-stimulated DAT internalization in both male and female VS. Further, these data reveal striking region- and sex-specific differences in PKC-regulated DAT trafficking, and its dependence upon Rit2.

Releasing the PKC-sensitive DAT endocytic brake drives DAT-Rit2 dissociation at the plasma membrane

Given that Rit2 stabilizes DAT surface levels and is required for PKC-stimulated trafficking, we next sought to decipher the molecular mechanisms by which Rit2 impacts DAT trafficking. We first asked whether driving DAT internalization, by disengaging the PKC-sensitive DAT endocytic brake, impacts the DAT-Rit2 interaction at the plasma membrane. To specifically interrogate the DAT surface population and its associated protein complex, we leveraged a bungarotoxin-binding site (BBS) strategy (Sekine-Aizawa and Huganir 2004; Wilkins, Li, and Smart 2008; Yang et al. 2010). We engineered a BBS into DAT extracellular loop 2, a site we previously successfully targeted for bioorthogonal DAT labeling (Wu et al. 2017), and which also tolerates an HA epitope (Sorkina et al. 2006). BBS-DAT expressed and functioned comparable to wt-DAT, and PKC activation acutely decreased BBS-DAT function to 67.97 ±5.9% control levels (Fig. 4A), which is comparable PKC-mediated DAT downregulation as previously reported by our group and others (Granas et al. 2003; Gorentla and Vaughan

2005; Navaroli et al. 2011; Bermingham and Blakely 2016; Wu et al. 2017). We first tested whether BBS-DAT could: 1) specifically isolate DAT via bungarotoxin labeling and pulldown, and 2) recover DAT-associated proteins. Cells expressing HA-Rit2 and either BBS-DAT or wt-DAT were labeled with biotinylated α-bungarotoxin (α-BTX-b), and DAT surface complexes were isolated by streptavidin pulldown. We specifically recovered BBS-DAT, but not wt-DAT, following α-BTX-b labeling (Fig. 4B). Importantly, Rit2 was recovered from pulldowns with BBS-DAT, but not in control pulldowns from cells expressing wt-DAT, demonstrating that Rit2 is recovered specifically following surface DAT pulldown. Additionally, BBS-DAT pulldowns did not recover the Rit2 homolog, Rit1 (Fig. 4C), consistent with a specific association between DAT and Rit2. We further asked whether other proteins required for PKC-mediated brake release are also part of the DAT surface complex. We previously reported that the non-receptor tyrosine kinase, Ack1 (TNK2) imposes the PKC-sensitive endocytic brake, and that PKC-mediated Ack1 inactivation is required for PKC-stimulated DAT internalization (Wu et al. 2015). However, it is not known whether Ack1 is associated with DAT at the plasma membrane. Following α-BTX-b labeling and pulldown, Ack1 was recovered from cells expressing BBS-DAT, but not from control cells expressing wt-DAT (Fig. 4D), demonstrating that Ack1 is part of the DAT surface complex. Thus, BBS-DAT has precise utility to interrogate surface DAT and its associated proteins, such as Rit2 and Ack1.

Given our previous imaging results (Navaroli et al. 2011), we hypothesized that PKC activation causes DAT and Rit2 to dissociate. Since PKC-stimulated DAT internalization can only occur when the endocytic brake is disengaged, we first leveraged BBS-DAT

pulldowns to ask whether PKC-mediated brake release alters the DAT-Rit2 surface association. PKC activation (1μM PMA, 30 min, 37°C) significantly decreased the DAT-Rit2 plasma membrane association (Fig. 5A). Additionally, DAT and Rit2 significantly dissociated when we directly released the DAT endocytic brake, by inactivating Ack1 with AIM-100 (20μM, 30 min, 37°C) (Fig. 5B). DAT and Rit2 may specifically dissociate at the cell surface in response to releasing the PKC-sensitive endocytic brake, or may do so following any stimulus that drives DAT internalization. To discern between these two possibilities, we measured the DAT-Rit2 surface association in response to AMPH exposure, which accelerates DAT internalization, but is Rho-dependent (Wheeler et al. 2015). In contrast to PKC-stimulated DAT-Rit2 dissociation, AMPH treatment (10μM, 30 min, 37°C) significantly increased the DAT-Rit2 surface association (Fig. 5C). Thus, the DAT-Rit2 surface dissociation occurs specifically when the PKC-sensitive DAT endocytic brake is disengaged, either in response to PKC activation or direct Ack1 inactivation, but is not a general result of accelerated DAT endocytosis.

The DAT amino terminus is integral to the DAT-Rit2 interaction and PKC-stimulated dissociation

The DAT-Rit2 interaction was originally identified in a yeast 2-hybrid screen, using DAT C-terminal residues 587-596 (FREKLAYAIA) as bait (Navaroli et al. 2011). However, it is not known which DAT domains are required (or sufficient) for the DAT-Rit2 association in the context of intact DAT protein, nor is it known whether any DAT domains are specifically required for PKC-stimulated DAT-Rit2 dissociation. Rit2 specifically binds DAT, but not SERT (Navaroli et al. 2011), thus we hypothesized that replacing DAT N- or C- termini with those of SERT may define DAT domains required

for Rit2 binding and/or PKC-stimulated DAT-Rit2 dissociation. To quantitatively assess whether either the DAT N- or C-terminus significantly impacts the DAT-Rit2 interaction, we performed live FRET imaging in cells co-transfected with YFP-Rit2 and either CFP-DAT or CFP-DAT/SERT chimeras, in which either the DAT N-, C-, or both termini were substituted with those of SERT, and which we previously characterized (Sweeney et al. 2017). As we previously reported, CFP-DAT and YFP-Rit2 elicited a significant FRET signal as compared to soluble YFP/CFP expression (Fig. 6A). Interestingly, replacing the DAT N-terminus with that of SERT (CFP-N-S/DAT) significantly increased the DAT-Rit2 interaction compared to CFP-DAT, whereas replacing the DAT C-terminus (CFP-DAT/C-S) or both termini (CFP-S/DAT/S) did not affect the DAT-Rit2 interaction (Fig. 6A). Consistent with these results, Rit2 was likewise recovered with BBS-tagged versions of each DAT/SERT chimera (Fig 6B). We next asked whether PKC-stimulated DAT-Rit2 dissociation requires either the DAT N- and/or C-terminus. Substituting the DAT C-terminus with that of SERT (DAT/C-S) had no significant effect on PKC-stimulated DAT-Rit2 dissociation, as compared to wt-DAT controls (Fig. 6C). However, substituting either the DAT N- terminus (N-S/DAT), or both N- and C- termini (S/DAT/S), with those of SERT abolished PKC-stimulated DAT-Rit2 dissociation (Fig 6C). Taken together, these results indicate that the DAT N-terminus is required for the PKC-stimulated DAT-Rit2 dissociation, and that the SERT N-terminus does not suffice. However, SERT N- and C- termini suffice to maintain the DAT-Rit2 association.

The DAT amino terminus is required for PKC-stimulated DAT internalization

Given that the DAT N-terminus is required for PKC-stimulated DAT-Rit2 dissociation, this raised the possibility that the N-terminus may also be required for stimulated DAT

internalization, mediated by either PKC stimulation or direct Ack1 inactivation. To test these possibilities, we measured DAT internalization rates in response to either PKC activation or direct Ack1 inactivation (with AIM-100) in stably-transfected SK-N-MC cells, in which we previously characterized both PKC- and AIM-100-stimulated DAT internalization (Gabriel et al. 2013; Wu et al. 2015). PKC activation (1μM PMA, 10 min, 37°C) significantly increased wt-DAT internalization, and substituting the DAT C-terminus with the SERT C-terminus (DAT/C-S) did not significantly affect PKC-stimulated internalization (Fig. 7A). However, PKC-stimulated DAT internalization was abolished when either the DAT N-terminus, or both N- and C-termini, were substituted with SERT termini (N-S/DAT and S/DAT/S, Fig. 7A). In contrast, direct Ack1 inactivation (20μM AIM-100, 10 min, 37°C) significantly stimulated wt-DAT, N-S/DAT, and DAT/C-S internalization, but had no effect on S/DAT/S internalization (Fig. 7A). To assure that these effects were not due to the lack of Rit2 expression in SK-N-MC cells, we further assessed basal and PKC-stimulated N-S/DAT internalization in stably transfected SK-N-DZ cells, which endogenously express Rit2. In SK-N-DZ cells, N-S/DAT internalized significantly slower than wt-DAT under basal conditions (Fig 7B). Additionally, while PKC activation significantly increased the wt-DAT internalization rate, it had no effect on N-S/DAT internalization as compared to its own vehicle control ($p=0.17$, one-way ANOVA with Bonferroni's multiple comparison test, $n=4-7$; Fig. 7B). These results demonstrate that the DAT N-terminus is required, and that the SERT N-terminus does not suffice, for PKC-stimulated DAT internalization.

Rit2 and Ack1 independently converge on DAT in response to PKC

We next asked whether there is a mechanistic relationship between Rit2, Ack1, and PKC-mediated release of the DAT endocytic brake. Rit2 may be upstream or downstream of Ack1 in the signaling cascade that leads from PKC to DAT. Alternatively, Rit2 and Ack1 may respond independently to PKC activation. We first used Rit2-KD in SK-N-DZ cells to ask whether Rit2 was required for PKC-mediated Ack1 inactivation, a requisite step for PKC-mediated release of the endocytic brake and for stimulated DAT internalization (Wu et al. 2015). In vector-transduced cells, PKC activation significantly reduced pY284-Ack1, to levels comparable to that achieved with the Ack1 inhibitor, AIM-100 (Fig. 8A). In cells transduced with shRIt2-107, pY284-pAck1 levels, were also significantly reduced in response to either PKC activation or AIM-100 treatment, and there was no difference in the magnitude change of pY284-pAck1 levels following PKC activation (Fig. 8A). These results indicate that Rit2 is not likely upstream of Ack1 in the signaling pathway that leads from PKC to Ack1 inactivation.

We next asked whether PKC-mediated Ack1 inactivation is required for, and therefore upstream of, PKC-stimulated DAT-Rit2 dissociation. To test this possibility, we measured DAT-Rit2 dissociation in cells co-transfected with DAT, Rit2, and either vector or the PKC-insensitive, constitutively active Ack1 mutant (S445P) which we previously reported blocks PKC-stimulated DAT internalization (Wu et al. 2015). In control cells, PKC activation drove a significant DAT-Rit2 dissociation (Fig. 8B). In cells co-transfected with S445P-Ack1, PKC activation likewise drove DAT-Rit2 dissociation, at levels indistinguishable from vector controls (Fig. 8B). These results demonstrate that PKC-stimulated DAT-Rit2 dissociation does not require Ack1 inactivation. Moreover, they demonstrate that even in conditions where DAT cannot internalize in response to

PKC activation (i.e. because Ack1 is constitutively active), PKC activation still drives DAT and Rit2 to dissociate. Thus, PKC-stimulated DAT-Rit2 dissociation is likely to occur prior to Ack1-mediated release of the DAT endocytic brake.

DISCUSSION

DAT is stabilized at the cell surface by a PKC-sensitive endocytic brake that requires 1) residues in both the DAT N- and C- termini to engage (Boudanova et al. 2008; Sorkina et al. 2009), and 2) Ack1 inactivation to release (Wu et al. 2015). Here, we found that Rit2 is required to release the PKC-sensitive DAT endocytic brake in cell lines and tissues where Rit2 is endogenously expressed, such as SK-N-DZ cells (Fig. 2C) and in VS (Fig. 3), respectively. Curiously, over two decades of evidence has demonstrated that PKC activation stimulates DAT internalization in multiple cell lines that apparently have a negligible amount, if any, Rit2 expression (Pristupa et al. 1998; Melikian and Buckley 1999; Daniels and Amara 1999; Sorkina et al. 2003; Sorkina et al. 2006) (Table 1). Given that Ack1 is ubiquitously expressed, we conclude that PKC-stimulated Ack1 inactivation can suffice to release the DAT endocytic brake in a heterologous context that may or may not express Rit2. However, when DAT is expressed in its appropriate context (i.e. striatal terminals), Rit2 expression is absolutely required for PKC-stimulated DAT internalization, and PKC-mediated Ack1 inactivation alone cannot suffice to release the endocytic brake (Fig. 3). These results further suggest that although Rit2 and Ack1 independently converge on DAT in response to PKC activation in cell lines (Fig. 8), there may be an, as of yet, unidentified DAergic-specific mechanism that facilitates a Rit2/Ack interdependence required for endocytic brake release.

Our previous study using total (i.e. not sub-dissected) striatal slices found that PKC activation decreased DAT surface expression by ~20% (Gabriel et al. 2013). Interestingly, in the current study, PKC activation drove ~35% DAT surface loss in both

male and female VS, but had no net effect on DAT surface expression in DS from either sex (Fig. 3). These data suggest that the somewhat modest PKC-stimulated DAT surface loss in total striatum reflects robust DAT surface loss in VS, which is diluted by the lack of any effect in DS. Is DAT endocytosis completely resistant to PKC activation in DS? It is currently unknown which PKC isoform(s) stimulate DAT internalization. We activated PKC with the phorbol ester PMA, which activates all diacylglycerol-sensitive PKC isoforms, including PKC-α, β1, β2, γ, and δ. PKCβ activity is required for D2 receptor-mediated DAT insertion into the plasma membrane, and selective PKCβ activation rapidly delivers DAT to the cell surface in both cell lines and striatal synaptosomes (Chen et al. 2013). Thus, it is possible that in DS, Rit2-dependent, PKC-stimulated DAT internalization may be countered by PKCβ-mediated DAT insertion, resulting in no detectable net change within the 30-min timeframe we tested. Indeed, following Rit2-KD, PKC activation increased DAT surface levels in male DS, consistent with PKCβ-mediated DAT insertion that is no longer counterbalanced by Rit2-dependent DAT internalization. In contrast to DS, DAT surface levels in VS were significantly decreased in response to PMA treatment, suggesting that the balance between PKCβ-mediated DAT insertion and Rit2-dependent DAT internalization may differ between DS and VS. A recent study, in which D2R activation increased DAT surface expression in the DS, but not VS, further supports this premise (Gowrishankar et al. 2018). Given that few studies, to date, have identified the receptor-mediated signaling pathways that lead to PKC-stimulated DAT internalization, nor the temporal profile of DAT response to PKC activation in DAergic terminals, it remains unclear how DAT insertion and internalization balance may occur.

In addition to regional differences in PKC-stimulated DAT internalization, we also found that DAergic Rit2 differentially impacts total DAT levels and DAT surface: intracellular in males and females, respectively (Fig. 3). We previously reported that Rit2-KD significantly reduced total striatal DAT protein levels in males, but not females (Sweeney et al. 2019). However, Rit2-KD had no effect on DAT surface: intracellular distribution in males. Thus, coupled with a decreased total DAT expression, Rit2-KD results in a net DAT loss at the surface in males. In females, Rit2-KD had no effect on total DAT, but decreased the DAT surface: intracellular distribution (Fig. 3), which also decreases absolute DAT surface levels. Therefore, although Rit2-KD imparts sex-specific effects on total DAT and DAT surface: intracellular distribution, the net effect in both sexes is decreased absolute DAT surface expression. This finding is somewhat unexpected, as it might be assumed that interfering with stimulated DAT internalization would likely tip the balance towards enhanced, rather than diminished, DAT surface expression. However, it is currently unknown to what extent DAT surface levels are fluctuating in real time, in response to the complex neurocircuitry within both the DS and VS, and whether any signaling pathways that converge on DAT may differentially rely upon Rit2 in males and females. Moreover, since we previously observed that Rit2-KD differentially impacted male and female acute cocaine responses (Sweeney et al. 2019), it is likewise tempting to speculate that this is due to sex-specific, Rit2-dependent DAT trafficking. Future studies probing sex-specific differences in DAT trafficking and regulation by native receptor activation should directly address these questions.

We used an extracellular BBS-tag to interrogate surface DAT and its associated protein complex. This approach was previously used successful by several groups (Sekine-

Aizawa and Huganir 2004; Bogdanov et al. 2006; Wilkins, Li, and Smart 2008), and has distinct advantages over immunological methods, since 1) the α-BTX/BBS affinity is significantly higher than that of antibody/antigen interactions, and 2) α-BTX/BBS binding is maintained in detergent lysates. Interestingly, although we observed significant DAT-Rit2 dissociation in response to releasing the PKC-sensitive DAT endocytic brake (Fig. 5), AMPH-stimulated DAT internalization increased the surface DAT-Rit2 population. Surface DAT is distributed among several membrane microdomains (Adkins et al. 2007; Navaroli et al. 2011; Cremona et al. 2011; Butler et al. 2015; Kovtun et al. 2015; Rahbek-Clemmensen et al. 2017; Thal et al. 2019; Lebowitz et al. 2019). Moreover, we previously reported that, 1) PKC activation preferentially depletes DAT from cholera toxin-positive (Ctx+) microdomains (Gabriel et al. 2013), and 2) there is significantly more DAT-Rit2 co-localization in Ctx+ microdomains (Navaroli et al. 2011). Conversely, AMPH treatment increases DAT localization to Ctx+ domains (Butler et al. 2015). Taken together, these results suggest that DAT may dissociate from Rit2, and internalize, preferentially from Ctx+ microdomains in response to PKC activation. In contrast, AMPH potentially drives DAT internalization from Ctx- domains, in which there is less DAT-Rit2 interaction, thereby leaving an enriched DAT-Rit2 population at the cell surface.

We originally identified the DAT-Rit2 interaction via a yeast 2-hybrid screen using the C-terminal DAT domain “FREKLAYAIA” as bait, and FRET studies revealed that Rit2 directly interacts with DAT, but not SERT, at the plasma membrane (Navaroli et al. 2011). However, the domains required for the DAT-Rit2 interaction, and their requirement for either PKC-stimulated DAT internalization or DAT-Rit2 dissociation were not defined. To address these questions, we used a series of DAT/SERT chimeras

previously reported by our lab (Sweeney et al. 2017), and found that the DAT N-terminus was required for PKC-stimulated DAT-Rit2 dissociation (Fig. 7). Indeed, under basal conditions, N-S/DAT and Rit2 interacted to a significantly higher degree than DAT-Rit2 controls (Fig. 6), consistent with a lack of DAT-Rit2 dissociation for the N-S/DAT chimera and higher steady-state interaction. N-S/DAT also basally internalized significantly slower than wt-DAT, consistent with its inability to disengage the endocytic brake. Moreover, DAT/C-S retained both Rit2 interaction and ability release the endocytic brake in response to PKC activation, suggesting that C-terminal determinants required for the DAT-Rit2 interaction are conserved in SERT. The FREKLAYAIA bait used in the yeast two-hybrid screen that revealed the DAT-Rit2 interaction is highly conserved across the SLC6 gene family (Holton, Loder, and Melikian 2005; Boudanova et al. 2008). Interestingly, although N-S/DAT was resistant to PKC-stimulated internalization, it retained AIM-100-dependent internalization, whereas S/DAT/S did not (Fig. 7), indicating that the DAT N-terminus is not required for direct Ack1-dependent endocytic brake release, and further supports the hypothesis that Rit2 and Ack1 converge on DAT independently in response to PKC activation. It should also be noted that we, and others, reported that AIM-100 also binds non-competitively to DAT (Wu et al. 2015; Sorkina et al. 2018), and recent reports suggest that AIM-100 can enhance DAT surface oligomerization (Sorkina et al. 2018; Cheng et al. 2019). Since both Ack1-dependent and AIM-100-stimulated internalization are specific for DAT, and not SERT, it is possible that S/DAT/S endocytic resistance to AIM-100 may be because the substituted SERT domains perturb the DAT/AIM-100 interaction. Likewise, it is possible

that the ability of N-S/DAT to internalize in response to AIM-100, but not PKC activation, may be due to a direct effect of AIM-100 on DAT.

In this study we present one of the first descriptions of region- and sex-dependent differences in DAT trafficking regulation. Furthermore, we greatly extend our knowledge of the mechanisms by which Rit2 governs DAT surface expression in bona fide DAergic terminals. Future studies that examine the cell autonomous endogenous signaling events that drive striatal DAT trafficking, and require Rit2, will shed further light on mechanisms that influence DA clearance and DA-dependent behaviors.

Acknowledgements: We thank Tucker L. Conklin for excellent technical support. This work was supported by NIH grants DA015169 (H.E.M), DA035224 (H.E.M), F31DA039592 (C.G.S), F31DA045446 (P.J.K), Austrian Science Foundation (FWF) F35-B06 (H.H.S), and the Swiss National Science Foundation P2BSP3_181809 (D.L.).

REFERENCES

Adkins, E. M., D. J. Samuvel, J. U. Fog, J. Eriksen, L. D. Jayanthi, C. B. Vaegter, S. Ramamoorthy, and U. Gether. 2007. 'Membrane mobility and microdomain association of the dopamine transporter studied with fluorescence correlation spectroscopy and fluorescence recovery after photobleaching', *Biochemistry*, 46: 10484-97.

Ashok, A. H., T. R. Marques, S. Jauhar, M. M. Nour, G. M. Goodwin, A. H. Young, and O. D. Howes. 2017. 'The dopamine hypothesis of bipolar affective disorder: the state of the art and implications for treatment', *Molecular Psychiatry*, 22: 666.

Bermingham, D. P., and R. D. Blakely. 2016. 'Kinase-dependent Regulation of Monoamine Neurotransmitter Transporters', *Pharmacol Rev*, 68: 888-953.

Bogdanov, Y., G. Michels, C. Armstrong-Gold, P. G. Haydon, J. Lindstrom, M. Pangalos, and S. J. Moss. 2006. 'Synaptic GABAA receptors are directly recruited from their extrasynaptic counterparts', *EMBO J*, 25: 4381-9.

Boudanova, E., D. M. Navaroli, Z. Stevens, and H. E. Melikian. 2008. 'Dopamine transporter endocytic determinants: carboxy terminal residues critical for basal and PKC-stimulated internalization', *Mol Cell Neurosci*, 39: 211-7.

Bowton, E., C. Saunders, I. A. Reddy, N. G. Campbell, P. J. Hamilton, L. K. Henry, H. Coon, D. Sakrikar, J. M. Veenstra-VanderWeele, R. D. Blakely, J. Sutcliffe, H. J. Matthies, K. Erreger, and A. Galli. 2014. 'SLC6A3 coding variant Ala559Val found in two autism probands alters dopamine transporter function and trafficking', *Transl Psychiatry*, 4: e464.

Burger, C., F. N. Nguyen, J. Deng, and R. J. Mandel. 2005. 'Systemic mannitol-induced hyperosmolality amplifies rAAV2-mediated striatal transduction to a greater extent than local co-infusion', *Mol Ther*, 11: 327-31.

Butler, B., K. Saha, T. Rana, J. P. Becker, D. Sambo, P. Davari, J. S. Goodwin, and H. Khoshbouei. 2015. 'Dopamine Transporter Activity Is Modulated by alpha-Synuclein', *J Biol Chem*, 290: 29542-54.

Chen, R., C. P. Daining, H. Sun, R. Fraser, S. L. Stokes, M. Leitges, and M. E. Gnegy. 2013. 'Protein kinase Cbeta is a modulator of the dopamine D2 autoreceptor-activated trafficking of the dopamine transporter', *J Neurochem*, 125: 663-72.

Cheng, M. H., L. Ponzoni, T. Sorkina, J. Y. Lee, S. Zhang, A. Sorkin, and I. Bahar. 2019. 'Trimerization of dopamine transporter triggered by AIM-100 binding: Molecular mechanism and effect of mutations', *Neuropharmacology*: 107676.

Cremona, M. L., H. J. Matthies, K. Pau, E. Bowton, N. Speed, B. J. Lute, M. Anderson, N. Sen, S. D. Robertson, R. A. Vaughan, J. E. Rothman, A. Galli, J. A. Javitch, and A. Yamamoto. 2011. 'Flotillin-1 is essential for PKC-triggered endocytosis and membrane microdomain localization of DAT', *Nat Neurosci*, 14: 469-77.

Daniels, G. M., and S. G. Amara. 1999. 'Regulated trafficking of the human dopamine transporter. Clathrin-mediated internalization and lysosomal degradation in response to phorbol esters', *J Biol Chem*, 274: 35794-801.

Eissa, Nermin, Mohammed Al-Houqani, Adel Sadeq, Shreesh K. Ojha, Astrid Sasse, and Bassem Sadek. 2018. 'Current Enlightenment About Etiology and Pharmacological Treatment of Autism Spectrum Disorder', *Frontiers in Neuroscience*, 12.

Emamalizadeh, B., J. Jamshidi, A. Movafagh, M. Ohadi, M. S. Khaniani, S. Kazeminasab, A. Biglarian, S. Taghavi, M. Motallebi, A. Fazeli, A. Ahmadifard, G. A. Shahidi, P. Petramfar, N. Shahmohammadibeni, T. Dadkhah, E. Khademi, A. Tafakhori, A. Khaligh, T. Safaralizadeh, A. Kowsari, A. Mirabzadeh, A. E. S. Zarneh, M. Khorrami, P. Shokraeian, M. J. S. Banavandi, B. S. Lima, M. Andarva, E. Alehabib, M. Atakhorrami,

and H. Darvish. 2017. 'RIT2 Polymorphisms: Is There a Differential Association?', *Mol Neurobiol*, 54: 2234-40.

Eriksen, J., W. E. Bjorn-Yoshimoto, T. N. Jorgensen, A. H. Newman, and U. Gether. 2010. 'Postendocytic sorting of constitutively internalized dopamine transporter in cell lines and dopaminergic neurons', *J Biol Chem*, 285: 27289-301.

Foo, J. N., L. C. Tan, I. D. Irwan, W. L. Au, H. Q. Low, K. M. Prakash, A. Ahmad-Annuar, J. Bei, A. Y. Chan, C. M. Chen, Y. C. Chen, S. J. Chung, H. Deng, S. Y. Lim, V. Mok, H. Pang, Z. Pei, R. Peng, H. F. Shang, K. Song, A. H. Tan, Y. R. Wu, T. Aung, C. Y. Cheng, F. T. Chew, S. H. Chew, S. A. Chong, R. P. Ebstein, J. Lee, S. M. Saw, A. Seow, M. Subramaniam, E. S. Tai, E. N. Vithana, T. Y. Wong, K. K. Heng, W. Y. Meah, C. C. Khor, H. Liu, F. Zhang, J. Liu, and E. K. Tan. 2017. 'Genome-wide association study of Parkinson's disease in East Asians', *Hum Mol Genet*, 26: 226-32.

Gabriel, L. R., S. Wu, P. Kearney, K. D. Bellve, C. Standley, K. E. Fogarty, and H. E. Melikian. 2013. 'Dopamine transporter endocytic trafficking in striatal dopaminergic neurons: differential dependence on dynamin and the actin cytoskeleton', *J Neurosci*, 33: 17836-46.

Gainetdinov, R. R., S. R. Jones, F. Fumagalli, R. M. Wightman, and M. G. Caron. 1998. 'Re-evaluation of the role of the dopamine transporter in dopamine system homeostasis', *Brain Res Brain Res Rev*, 26: 148-53.

Geibl, Fanni F., Martin T. Henrich, and Wolfgang H. Oertel. 2019. 'Mesencephalic and extramesencephalic dopaminergic systems in Parkinson’s disease', *Journal of Neural Transmission*.

Giros, B., M. Jaber, S. R. Jones, R. M. Wightman, and M. G. Caron. 1996. 'Hyperlocomotion and indifference to cocaine and amphetamine in mice lacking the dopamine transporter', *Nature*, 379: 606-12.

Glessner, J. T., M. P. Reilly, C. E. Kim, N. Takahashi, A. Albano, C. Hou, J. P. Bradfield, H. Zhang, P. M. Sleiman, J. H. Flory, M. Imielinski, E. C. Frackelton, R. Chiavacci, K. A. Thomas, M. Garris, F. G. Otieno, M. Davidson, M. Weiser, A. Reichenberg, K. L. Davis, J. I. Friedman, T. P. Cappola, K. B. Margulies, D. J. Rader, S. F. Grant, J. D. Buxbaum, R. E. Gur, and H. Hakonarson. 2010. 'Strong synaptic transmission impact by copy number variations in schizophrenia', *Proc Natl Acad Sci U S A*, 107: 10584-9.

Gorentla, B. K., and R. A. Vaughan. 2005. 'Differential effects of dopamine and psychoactive drugs on dopamine transporter phosphorylation and regulation', *Neuropharmacology*, 49: 759-68.

Gowrishankar, R., P. J. Gresch, G. L. Davis, R. M. Katamish, J. R. Riele, A. M. Stewart, R. A. Vaughan, M. K. Hahn, and R. D. Blakely. 2018. 'Region-Specific Regulation of Presynaptic Dopamine Homeostasis by D2 Autoreceptors Shapes the In Vivo Impact of the Neuropsychiatric Disease-Associated DAT Variant Val559', *J Neurosci*, 38: 5302-12.

Granas, C., J. Ferrer, C. J. Loland, J. A. Javitch, and U. Gether. 2003. 'N-terminal truncation of the dopamine transporter abolishes phorbol ester- and substance P receptor-stimulated phosphorylation without impairing transporter internalization', *J Biol Chem*, 278: 4990-5000.

Hamedani, S. Y., J. Gharesouran, R. Noroozi, A. Sayad, M. D. Omrani, A. Mir, S. S. A. Afjeh, M. Toghi, S. Manoochehrabadi, S. Ghafouri-Fard, and M. Taheri. 2017. 'Ras-like without CAAX 2 (RIT2): a susceptibility gene for autism spectrum disorder', *Metab Brain Dis*, 32: 751-55.

Hamilton, P. J., N. G. Campbell, S. Sharma, K. Erreger, F. Herborg Hansen, C. Saunders, A. N. Belovich, Nih Arra Autism Sequencing Consortium, M. A. Sahai, E. H. Cook, U. Gether, H. S. McHaourab, H. J. Matthies, J. S. Sutcliffe, and A. Galli. 2013. 'De novo mutation in the dopamine transporter gene associates dopamine dysfunction with autism spectrum disorder', *Mol Psychiatry*, 18: 1315-23.

Heo, W. D., T. Inoue, W. S. Park, M. L. Kim, B. O. Park, T. J. Wandless, and T. Meyer. 2006. 'PI(3,4,5)P3 and PI(4,5)P2 lipids target proteins with polybasic clusters to the plasma membrane', *Science*, 314: 1458-61.

Herborg, F., T. F. Andreassen, F. Berlin, C. J. Loland, and U. Gether. 2018. 'Neuropsychiatric disease-associated genetic variants of the dopamine transporter display heterogeneous molecular phenotypes', *J Biol Chem*, 293: 7250-62.

Holton, K. L., M. K. Loder, and H. E. Melikian. 2005. 'Nonclassical, distinct endocytic signals dictate constitutive and PKC-regulated neurotransmitter transporter internalization', *Nat Neurosci*, 8: 881-8.

Howes, Oliver D., Robert McCutcheon, Michael J. Owen, and Robin M. Murray. 2017. 'The Role of Genes, Stress, and Dopamine in the Development of Schizophrenia', *Biological Psychiatry*, 81: 9-20.

Hyman, Steven E., Robert C. Malenka, and Eric J. Nestler. 2006. 'Neural Mechanisms of Addiction: The Role of Reward-Related Learning and Memory', *Annual Review of Neuroscience*, 29: 565-98.

Iversen, S. D., and L. L. Iversen. 2007. 'Dopamine: 50 years in perspective', *Trends Neurosci*, 30: 188-93.

Kovtun, O., D. Sakrikar, I. D. Tomlinson, J. C. Chang, X. Arzeta-Ferrer, R. D. Blakely, and S. J. Rosenthal. 2015. 'Single-quantum-dot tracking reveals altered membrane dynamics of an attention-deficit/hyperactivity-disorder-derived dopamine transporter coding variant', *ACS Chem Neurosci*, 6: 526-34.

Kristensen, Anders S., Jacob Andersen, Trine N. Jørgensen, Lena Sørensen, Jacob Eriksen, Claus J. Loland, Kristian Strømgaard, and Ulrik Gether. 2011. 'SLC6 Neurotransmitter Transporters: Structure, Function, and Regulation', *Pharmacological Reviews*, 63: 585-640.

Kume, K., S. Kume, S. K. Park, J. Hirsh, and F. R. Jackson. 2005. 'Dopamine is a regulator of arousal in the fruit fly', *J Neurosci*, 25: 7377-84.

Kurian, M. A., J. Zhen, S. Y. Cheng, Y. Li, S. R. Mordekar, P. Jardine, N. V. Morgan, E. Meyer, L. Tee, S. Pasha, E. Wassmer, S. J. Heales, P. Gissen, M. E. Reith, and E. R. Maher. 2009. 'Homozygous loss-of-function mutations in the gene encoding the dopamine transporter are associated with infantile parkinsonism-dystonia', *J Clin Invest*, 119: 1595-603.

Lebowitz, J. J., J. A. Pino, P. M. Mackie, M. Lin, C. Hurst, K. Divita, A. T. Collins, D. N. Koutzoumis, G. E. Torres, and H. Khoshbouei. 2019. 'Clustered Kv2.1 decreases dopamine transporter activity and internalization', *J Biol Chem*.

Lee, C. H., N. G. Della, C. E. Chew, and D. J. Zack. 1996. 'Rin, a neuron-specific and calmodulin-binding small G-protein, and Rit define a novel subfamily of ras proteins', *J Neurosci*, 16: 6784-94.

Loder, M. K., and H. E. Melikian. 2003. 'The dopamine transporter constitutively internalizes and recycles in a protein kinase C-regulated manner in stably transfected PC12 cell lines', *J Biol Chem*, 278: 22168-74.

Mazei-Robison, M. S., and R. D. Blakely. 2005. 'Expression studies of naturally occurring human dopamine transporter variants identifies a novel state of transporter inactivation associated with Val382Ala', *Neuropharmacology*, 49: 737-49.

Melikian, H. E. 2004. 'Neurotransmitter transporter trafficking: endocytosis, recycling, and regulation', *Pharmacol Ther*, 104: 17-27.

Melikian, H. E., and K. M. Buckley. 1999. 'Membrane trafficking regulates the activity of the human dopamine transporter', *J Neurosci*, 19: 7699-710.

Mueller, C., D. Ratner, L. Zhong, M. Esteves-Sena, and G. Gao. 2012. 'Production and discovery of novel recombinant adeno-associated viral vectors', *Curr Protoc Microbiol*, Chapter 14: Unit14D 1.

Navaroli, D. M., Z. H. Stevens, Z. Uzelac, L. Gabriel, M. J. King, L. M. Lifshitz, H. H. Sitte, and H. E. Melikian. 2011. 'The plasma membrane-associated GTPase Rin interacts with the dopamine transporter and is required for protein kinase C-regulated dopamine transporter trafficking', *J Neurosci*, 31: 13758-70.

Ng, J., J. Zhen, E. Meyer, K. Erreger, Y. Li, N. Kakar, J. Ahmad, H. Thiele, C. Kubisch, N. L. Rider, D. H. Morton, K. A. Strauss, E. G. Puffenberger, D. D'Agnano, Y. Anikster, C. Carducci, K. Hyland, M. Rotstein, V. Leuzzi, G. Borck, M. E. Reith, and M. A. Kurian. 2014. 'Dopamine transporter deficiency syndrome: phenotypic spectrum from infancy to adulthood', *Brain*, 137: 1107-19.

Pankratz, N., G. W. Beecham, A. L. DeStefano, T. M. Dawson, K. F. Doheny, S. A. Factor, T. H. Hamza, A. Y. Hung, B. T. Hyman, A. J. Ivinson, D. Krainc, J. C. Latourelle, L. N. Clark, K. Marder, E. R. Martin, R. Mayeux, O. A. Ross, C. R. Scherzer, D. K. Simon, C. Tanner, J. M. Vance, Z. K. Wszolek, C. P. Zabetian, R. H. Myers, H. Payami, W. K. Scott, T. Foroud, and Pd Gwas Consortium. 2012. 'Meta-analysis of Parkinson's disease: identification of a novel locus, RIT2', *Ann Neurol*, 71: 370-84.

Pristupa, Z. B., F. McConkey, F. Liu, H. Y. Man, F. J. Lee, Y. T. Wang, and H. B. Niznik. 1998. 'Protein kinase-mediated bidirectional trafficking and functional regulation of the human dopamine transporter', *Synapse*, 30: 79-87.

Rahbek-Clemmensen, T., M. D. Lycas, S. Erlendsson, J. Eriksen, M. Apuschkin, F. Vilhardt, T. N. Jorgensen, F. H. Hansen, and U. Gether. 2017. 'Super-resolution microscopy reveals functional organization of dopamine transporters into cholesterol and neuronal activity-dependent nanodomains', *Nat Commun*, 8: 740.

Sakrikar, D., M. S. Mazei-Robison, M. A. Mergy, N. W. Richtand, Q. Han, P. J. Hamilton, E. Bowton, A. Galli, J. Veenstra-Vanderweele, M. Gill, and R. D. Blakely. 2012. 'Attention deficit/hyperactivity disorder-derived coding variation in the dopamine transporter disrupts microdomain targeting and trafficking regulation', *J Neurosci*, 32: 5385-97.

Sekine-Aizawa, Y., and R. L. Huganir. 2004. 'Imaging of receptor trafficking by using alpha-bungarotoxin-binding-site-tagged receptors', *Proc Natl Acad Sci U S A*, 101: 17114-9.

Sharma, Alok, and Justin Couture. 2014. 'A Review of the Pathophysiology, Etiology, and Treatment of Attention-Deficit Hyperactivity Disorder (ADHD)', *Annals of Pharmacotherapy*, 48: 209-25.

Shi, G. X., J. Han, and D. A. Andres. 2005. 'Rin GTPase couples nerve growth factor signaling to p38 and b-Raf/ERK pathways to promote neuronal differentiation', *J Biol Chem*, 280: 37599-609.

Sorkina, T., S. Doolen, E. Galperin, N. R. Zahniser, and A. Sorkin. 2003. 'Oligomerization of dopamine transporters visualized in living cells by fluorescence resonance energy transfer microscopy', *J Biol Chem*, 278: 28274-83.

Sorkina, T., S. Ma, M. B. Larsen, S. C. Watkins, and A. Sorkin. 2018. 'Small molecule induced oligomerization, clustering and clathrin-independent endocytosis of the dopamine transporter', *Elife*, 7.

Sorkina, T., M. Miranda, K. R. Dionne, B. R. Hoover, N. R. Zahniser, and A. Sorkin. 2006. 'RNA interference screen reveals an essential role of Nedd4-2 in dopamine transporter ubiquitination and endocytosis', *J Neurosci*, 26: 8195-205.

Sorkina, T., T. L. Richards, A. Rao, N. R. Zahniser, and A. Sorkin. 2009. 'Negative regulation of dopamine transporter endocytosis by membrane-proximal N-terminal residues', *J Neurosci*, 29: 1361-74.

Sweeney, C. G., P. J. Kearney, R. R. Fagan, L. A. Smith, N. C. Bolden, R. Zhao-Shea, I. V. Rivera, J. Kolpakova, J. Xie, G. Gao, A. R. Tapper, G. E. Martin, and H. E. Melikian. 2019. 'Conditional, inducible gene silencing in dopamine neurons reveals a sex-specific role for Rit2 GTPase in acute cocaine response and striatal function', *Neuropsychopharmacology*.

Sweeney, C. G., B. P. Tremblay, T. Stockner, H. H. Sitte, and H. E. Melikian. 2017. 'Dopamine Transporter Amino and Carboxyl Termini Synergistically Contribute to Substrate and Inhibitor Affinities', *J Biol Chem*, 292: 1302-09.

Thal, L. B., I. D. Tomlinson, M. A. Quinlan, O. Kovtun, R. D. Blakely, and S. J. Rosenthal. 2019. 'Single Quantum Dot Imaging Reveals PKCbeta-Dependent Alterations in Membrane Diffusion and Clustering of an Attention-Deficit Hyperactivity Disorder/Autism/Bipolar Disorder-Associated Dopamine Transporter Variant', *ACS Chem Neurosci*, 10: 460-71.

Uenaka, T., W. Satake, P. C. Cha, H. Hayakawa, K. Baba, S. Jiang, K. Kobayashi, M. Kanagawa, Y. Okada, H. Mochizuki, and T. Toda. 2018. 'In silico drug screening by using genome-wide association study data repurposed dabrafenib, an anti-melanoma drug, for Parkinson's disease', *Hum Mol Genet*, 27: 3974-85.

Wes, P. D., M. Yu, and C. Montell. 1996. 'RIC, a calmodulin-binding Ras-like GTPase', *EMBO J*, 15: 5839-48.

Wheeler, D. S., S. M. Underhill, D. B. Stolz, G. H. Murdoch, E. Thiels, G. Romero, and S. G. Amara. 2015. 'Amphetamine activates Rho GTPase signaling to mediate dopamine transporter internalization and acute behavioral effects of amphetamine', *Proc Natl Acad Sci U S A*, 112: E7138-47.

Wilkins, M. E., X. Li, and T. G. Smart. 2008. 'Tracking cell surface GABAB receptors using an alpha-bungarotoxin tag', *J Biol Chem*, 283: 34745-52.

Wise, R. A. 2004. 'Dopamine, learning and motivation', *Nat Rev Neurosci*, 5: 483-94.

Wu, S., K. D. Bellve, K. E. Fogarty, and H. E. Melikian. 2015. 'Ack1 is a dopamine transporter endocytic brake that rescues a trafficking-dysregulated ADHD coding variant', *Proc Natl Acad Sci U S A*, 112: 15480-5.

Wu, S., R. R. Fagan, C. Uttamapinant, L. M. Lifshitz, K. E. Fogarty, A. Y. Ting, and H. E. Melikian. 2017. 'The Dopamine Transporter Recycles via a Retromer-Dependent Postendocytic Mechanism: Tracking Studies Using a Novel Fluorophore-Coupling Approach', *J Neurosci*, 37: 9438-52.

Yang, T., X. Xu, T. Kernan, V. Wu, and H. M. Colecraft. 2010. 'Rem, a member of the RGK GTPases, inhibits recombinant CaV1.2 channels using multiple mechanisms that require distinct conformations of the GTPase', *J Physiol*, 588: 1665-81.

Zhang, L., k. Wahlin, Y. Li, T. Masuda, Z. Yang, D. J. Zack, and N. Esumi. 2013. 'RIT2, a neuron-specific small guanosine triphosphatase, is expressed in retinal neuronal cells and its promoter is modulated by the POU4 transcription factors', *Molecular Vision*, 19: 1371-86.

Zhang, X., M. Niu, H. Li, and A. Xie. 2015. 'RIT2 rs12456492 polymorphism and the risk of Parkinson's disease: A meta-analysis', *Neurosci Lett*, 602: 167-71.

Zhou, Q., J. Li, H. Wang, Y. Yin, and J. Zhou. 2011. 'Identification of nigral dopaminergic neuron-enriched genes in adult rats', *Neurobiol Aging*, 32: 313-26.

Table I. *Rit2 expression in mammalian cell lines and brain regions*
Rit2 mRNA expression was determined by RT-qPCR and normalized to internal GAPDH values. n = 2-4

Species/Cell line	Rit2 ($2^{-\Delta Ct}$x10^4 ±S.E.M)
Mouse	
CAD	0.02 ±0.0067
N2a	0.09 ±0.052
NIH/3T3	No signal detected
Mouse Midbrain	72.0 ±12.8
Mouse Cortex	54.8 ±9.19
Rat	
AN27	No signal detected
PC12	No signal detected
Rat Midbrain	1100.0 ±0.51
Human	
HEK293T	0.40 ±0.34
SH-SY5Y	1.3 ± 0.56
SK-N-MC	0.09 ±0.07
SK-N-DZ	27.2 ±18.7

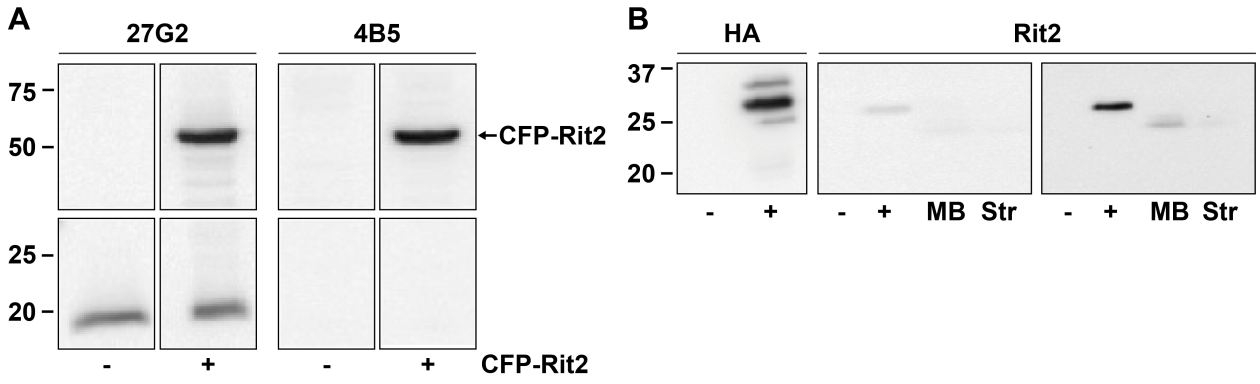

Figure 1. Rit2 protein is specifically detected by clone 4B5, but not clone 27G2, anti-Rit2 antibodies. A. HEK293T cells were transfected with either vector (-) or CFP-Rit2 (+) and cell lysates were assessed by immunoblot 48 hrs. post-transfection, probing with either anti-Rit2 clones 27G2 (left) or 4B5 (right) as described in *Materials and Methods*. Molecular weight markers indicate kDa. Clone 4B5 only detected a band from CFP-Rit2-transfected cells. **B.** HEK293T cells transfected with vector (-) or HA-Rit2 (+), mouse midbrain (MB), and mouse striatum (Str), were assessed by immunoblot, probing with either anti-HA (left) or anti-Rit2 clone 4B5. Note that both short (10 seconds; middle panel) and long (5 min; right panel) exposures of the same lanes are presented. Anti-Rit2 clone 4B5 detects an immunoreactive band in midbrain and striatum with higher mobility than HA-Rit2 expressed in HEK293T cells.

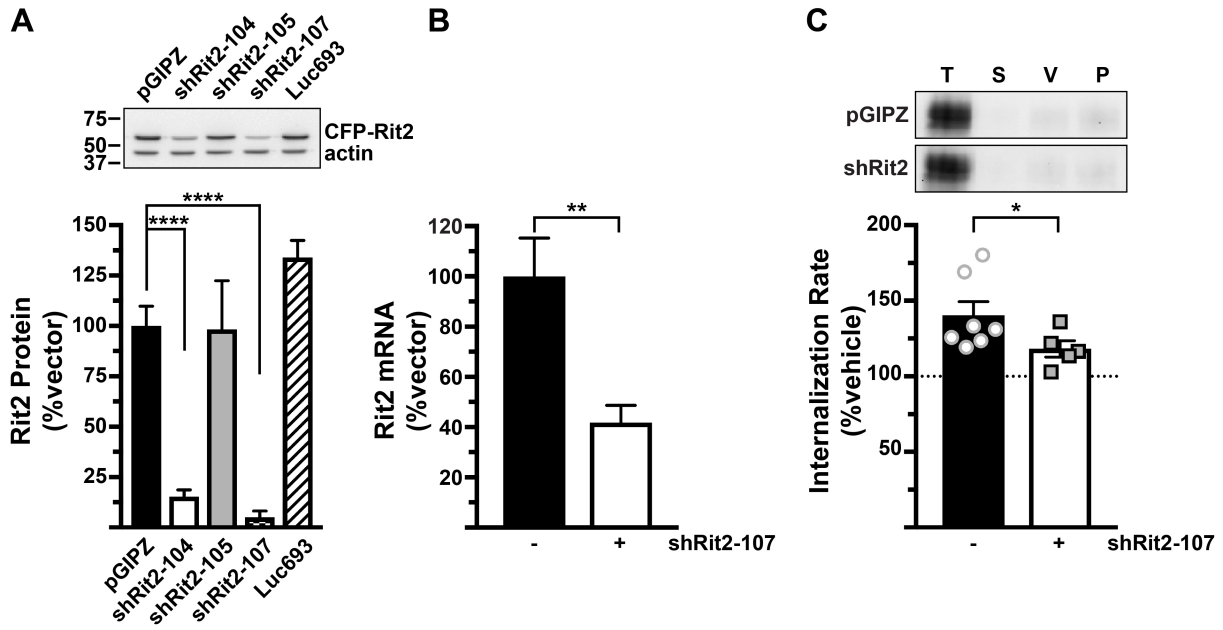

Figure 2. Rit2 is required for PKC-stimulated DAT internalization in DAT-SK-N-DZ cells. A. *human Rit2 shRNA screen*. Mouse N2a cells were co-transfected with human CFP-Rit2, and either pGIPZ vector, luciferase293 control, or Rit2 shRNA constructs. *Top*: Representative immunoblots. *Bottom*: Average CFP-Rit2 levels, normalized to actin loading controls, expressed as %pGIPZ control ±SEM. ****Significantly different from vector control, $p<0.0001$, one-way ANOVA with Dunnett's post-hoc comparison, n=3-5. **B.** *shRit2-mediated knockdown in stable DAT-SK-N-DZ cells*. DAT-SK-N-DZ cells were transduced with lentiviral particles expressing either pGIPZ or shRit2-107, and Rit2 expression was determined by RT-qPCR 96 hrs post-transduction. Average $\Delta\Delta$Ct values are presented, expressed as %vector-transduced values ±SEM. **$p=0.002$, two-tailed Student's t test, n=5. **C**. *DAT Internalization assay*. Stable DAT-SK-N-DZ cells were transduced with the indicated lentiviral particles and DAT internalization rates were measured 96 hrs post-transduction as described in *Materials and Methods*. *Top*: Representative immunoblots depicting surface DAT expression at t=0 (T), strip control (S), and internalized DAT during either vehicle (V) or 1 μM PMA (P) treatment. *Bottom*: Average DAT internalization rates expressed as %vehicle-treated control rates ±SEM. *$p=0.04$, one-tailed Student's t test, n=5-7.

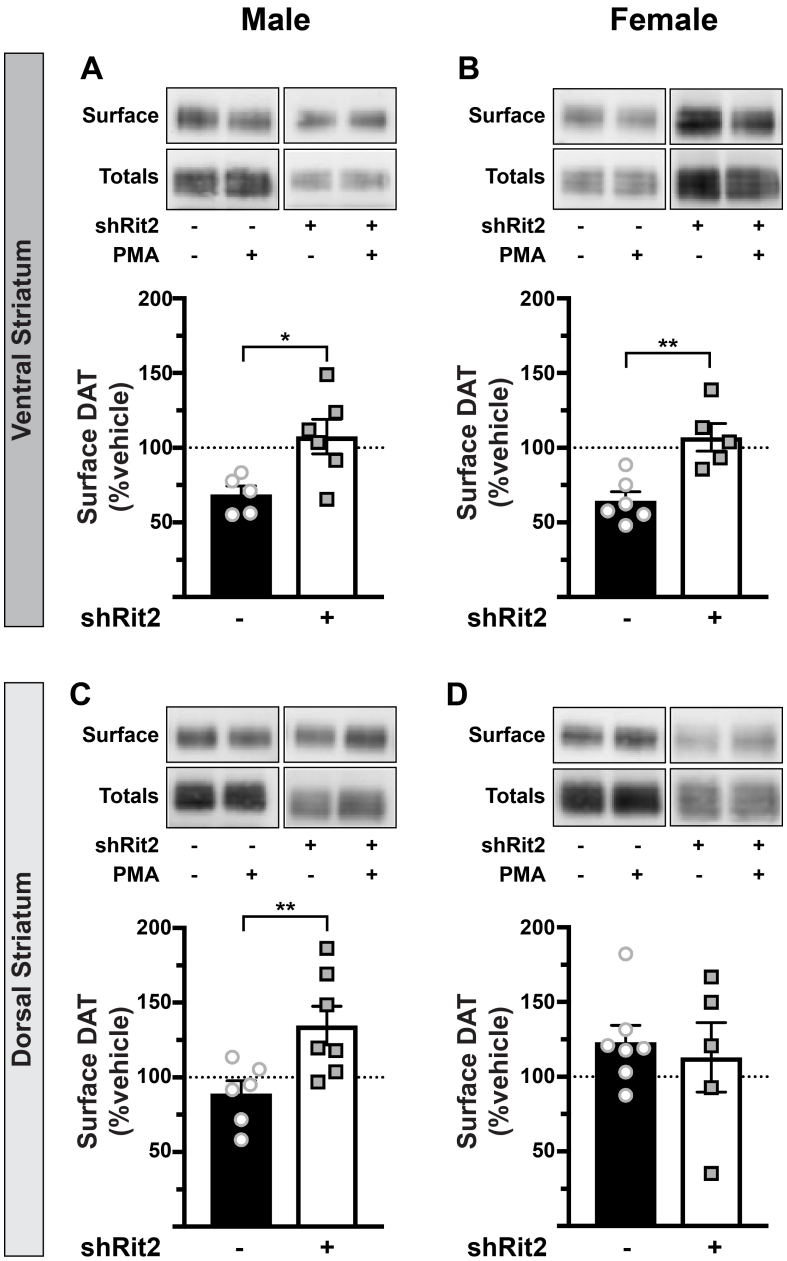

Figure 3. PKC-induced DAT internalization in mouse DAergic terminals requires Rit2 in a region- and sex-specific manner. *Conditional Rit2 silencing in DA neurons and ex vivo striatal slice biotinylation*. Male and female *Pitx3*$^{IRES2\text{-}tTA/+}$ mice VTA were bilaterally injected with either AAV9-TRE-GFP or -shRit2. Brains were harvested 4-5 weeks post-injection, and DAT surface expression was measured in *ex vivo* striatal slices by surface biotinylation as described in *Materials and Methods,* following treatment ±1μM PMA, 30 min, 37°C. Representative blots are shown in the top of each panel, and average data are presented at the bottom of each panel. DAT surface levels are expressed as %vehicle-treated, contralateral hemi-slice values, ±S.E.M. All data were evaluated using two-tailed Student's t test, n=5-7 slices from n=3 independent mice/virus. **A, B.** *Ventral striatum*. Rit2-KD significantly blocked PKC-stimulated DAT internalization in ventral striatum in males (**A,** *p=0.01) and females (**B**, **p=0.002). **C, D.** *Dorsal striatum.* In males, PKC activation had no effect on DAT surface levels in either control males (**C)** or females (**D**). Rit2-KD led to PKC-stimulated DAT surface increase and males **(C, **p=0.008), whereas PKC had no effect on DAT surface levels in females (p=0.34).

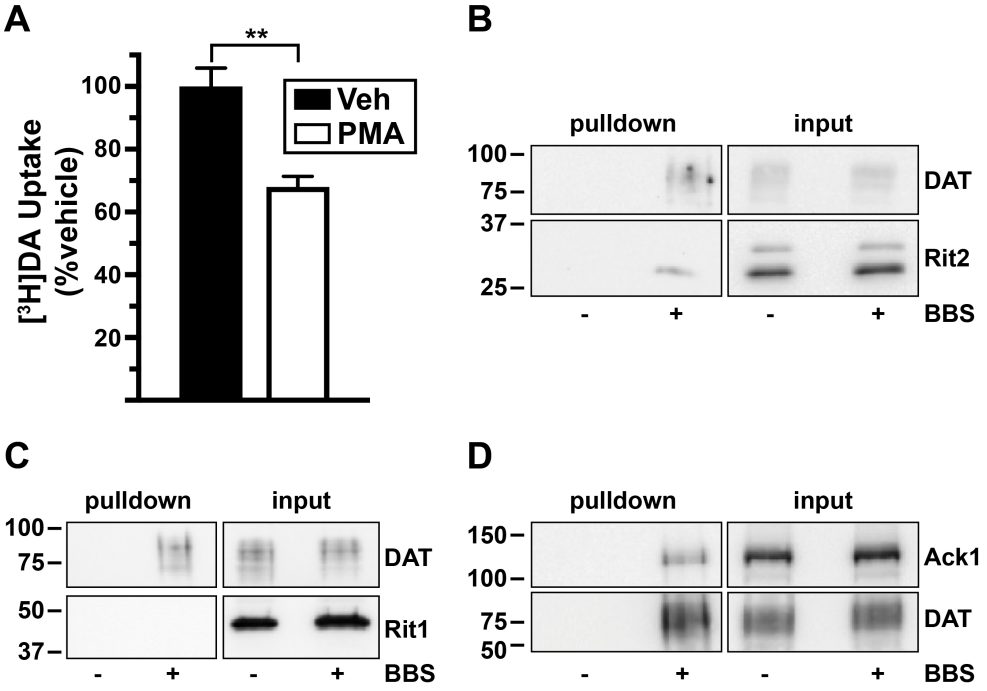

Figure 4. Surface DAT associates with Rit2 and Ack1, but not Rit1. **A**. *[^{3}H]DA uptake assay.* Cells expressing BBS-DAT were treated ±1μM PMA, 30 min, 37°C and [^{3}H]DA uptake was measured as described in *Materials and Methods*. Average data are expressed as %vehicle-treated specific [^{3}H]DA uptake ±SEM. **p=0.0045, two-tailed Student's t test, n=3. **B-D**. *BBS-DAT pulldowns*. Cells were co-transfected with DAT (±BBS tag), and either HA-Rit2 **(B)**, GFP-Rit1 **(C)**, or Ack1-HA **(D)** and DAT surface complexes were recovered by streptavidin pulldown as described in *Materials and Methods.* Both pull-down (left panels) and their respective ¼ input (right panels) immunoblots are presented and are representative of 3 independent experiments. **B.** Rit2 was specifically recovered in pulldowns from BBS-, but not wt-DAT. **C**. The Rit2 homolog, Rit1, was not recovered in DAT surface complexes. **D**. Ack1 was recovered from BBS-DAT pulldowns.

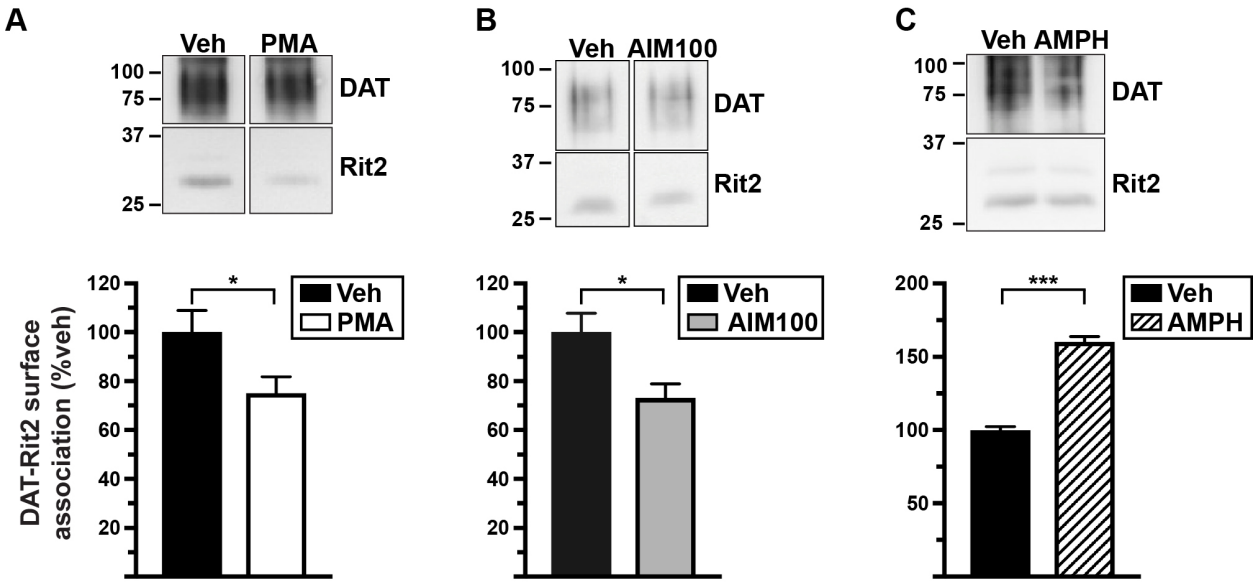

Figure 5. PKC activation drives DAT-Rit2 dissociation at the plasma membrane. *BBS-DAT pull-downs*. HEK293T cells were co-transfected with BBS-DAT and HA-Rit2, were treated with the indicated drugs, 30 min, 37°C, labeled with α-BTX-b, and DAT surface complexes were isolated as described in *Materials and Methods. Top panels*: Representative immunoblots. *Bottom panels:* Average DAT-Rit2 association expressed as %vehicle-treated control ±SEM, and were assessed by two-tailed Student's t test. **A.** PKC activation significantly decreased the DAT-Rit2 surface association, *p=0.04, n=6. **B**. Ack1 inactivation with AIM-100 decreased the DAT-Rit2 surface association, *p=0.03, n=4. **C**. AMPH treatment significantly increased DAT-Rit2 surface association, ***p=0.002, n=3.

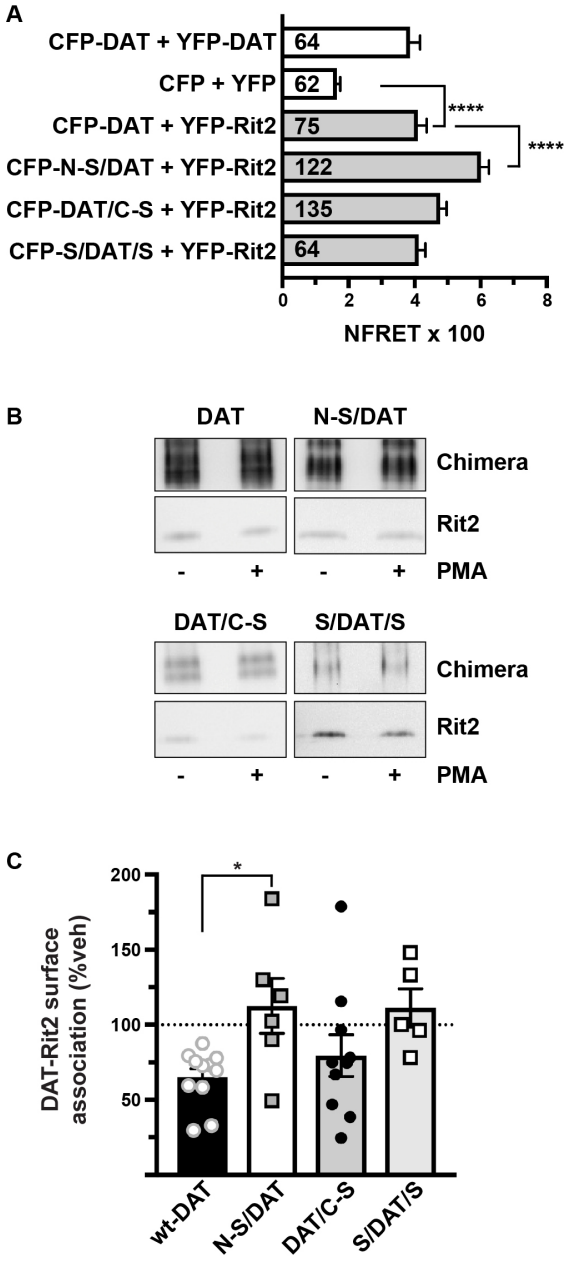

Figure 6. The SERT N-terminus promotes the DAT-Rit2 interaction and blocks PKC-stimulated DAT-Rit2 dissociation. A. *FRET studies.* HEK293 cells were transfected with the indicated plasmids and surface FRET measurements were made 24 hrs. post-transfection, as described in *Materials and Methods.* Average NFRET values (x100) for the indicated pairs are presented. ****Significantly different from CFP-DAT/YFP-Rit2 signal, Kruskal-Wallis test with Dunn's multiple comparisons test, $p<0.0001$, N values are provided within each bar. **B, C.** *BBS-DAT pull-downs.* HEK293T cells were co-transfected with HA-Rit2 and the indicated BBS-tagged proteins. Cells were treated ±1μM PMA, 30 min, 37°C, surface-labeled with α-BTX-b and DAT surface complexes were recovered by streptavidin pulldown as described in *Materials and Methods*. **B**. Representative immunoblots. **C**. Average data, presented as %vehicle-treated DAT-Rit2 association for each indicated protein. *Significantly different from wt-DAT control, one-way ANOVA with Dunnett's multiple comparison test, $p=0.03$, n=5-11.

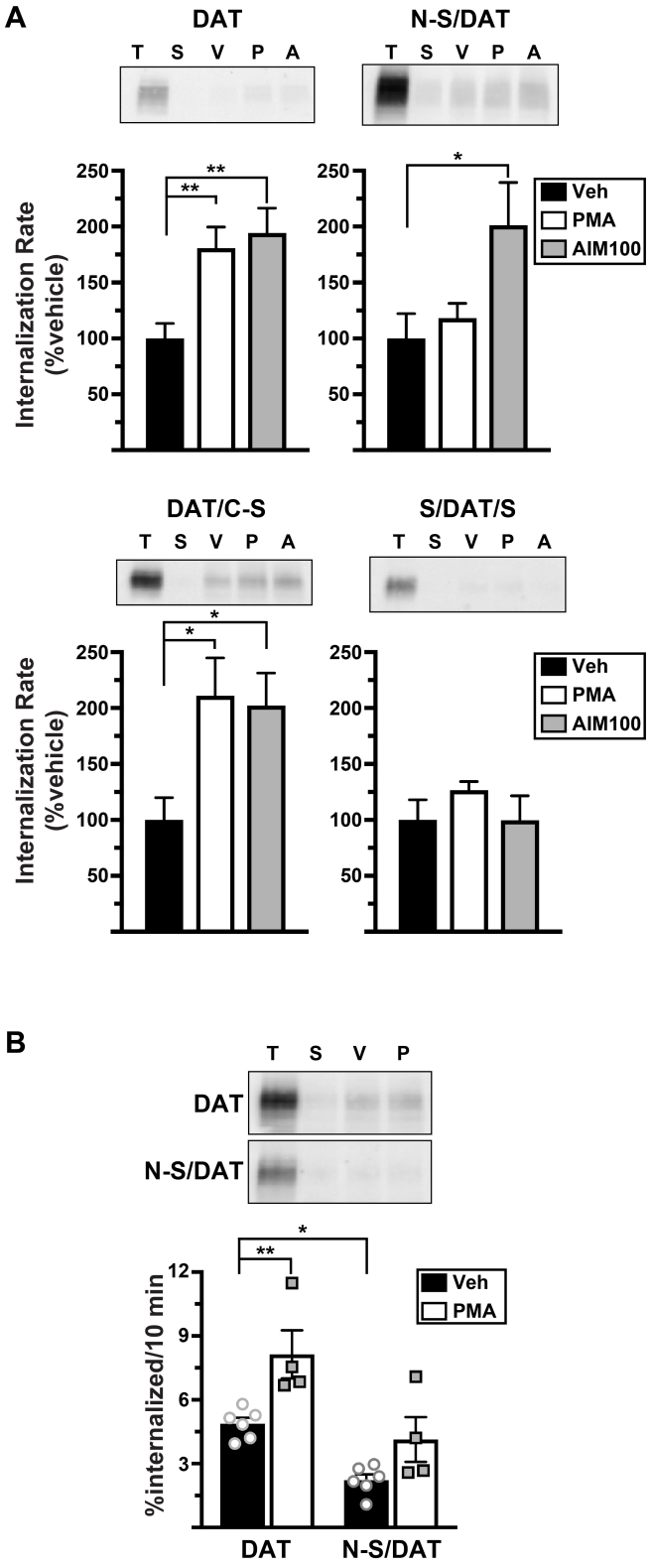

Figure 7. The DAT N-terminus is required for PKC-stimulated internalization. *DAT Internalization assays*. Wt-DAT and DAT/SERT chimera internalization rates were measured ±1μM PMA or ±20μM AIM-100, 10 min, 37°C, as described in *Materials and Methods. Tops:* Representative immunoblots showing total surface expression at t=0 (T), strip control (S), and internalized protein during vehicle (V), and PMA (P) treatments for the indicated proteins. *Bottoms:* Averaged data. **A**. Stable SK-N-MC cell lines. Average internalization rates, expressed as %vehicle-treated control rates ±SEM. Asterisks indicate a significant difference from each protein's respective control. *p<0.05, **p<0.01, one-way ANOVA with Dunnett's multiple comparison test, n=8-13. **B.** Stable SK-N-DZ cell lines. Average internalization rates are expressed as %surface protein internalized/10 min, ±SEM. Asterisks indicate a significant difference from the indicated protein or treatment. *p<0.05, **p<0.01, one-way ANOVA with Bonferroni's multiple comparison test, n=4-7.

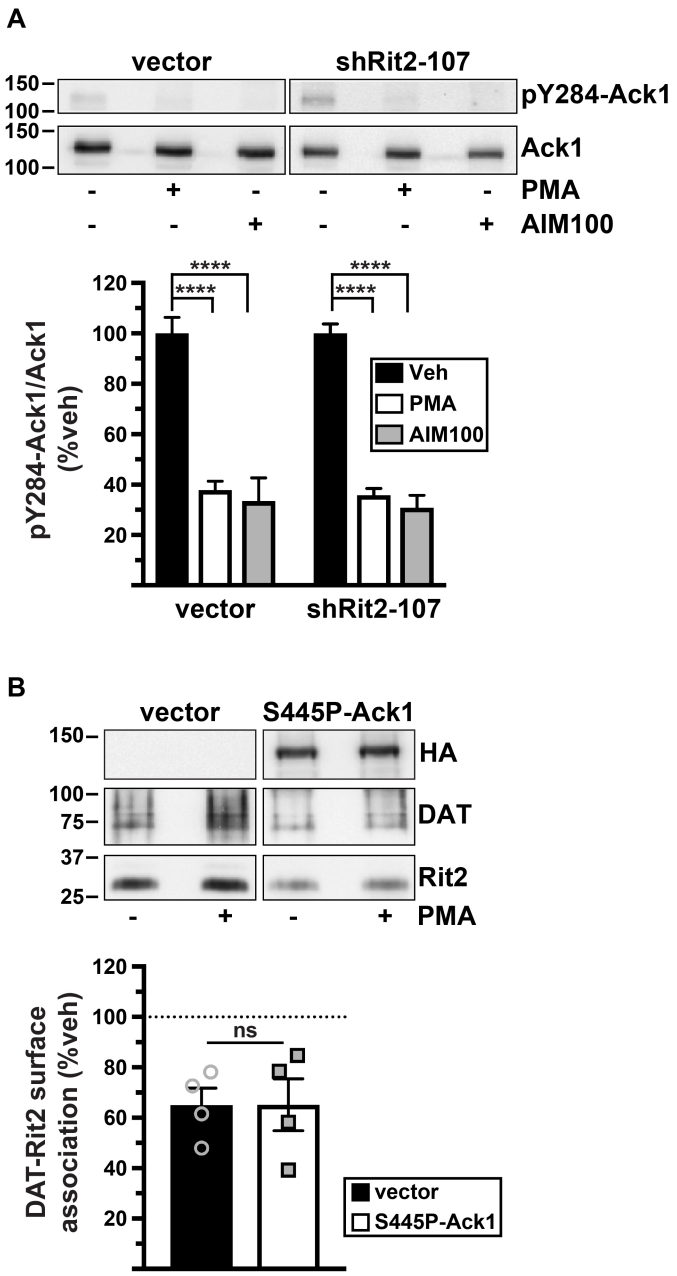

Figure 8. Rit2 and Ack1 independently converge on DAT in response to PKC activation. A. *Effect of Rit2 silencing on PKC-mediated Ack1 inactivation*. SK-N-DZ cells transduced with lentiviral particles expressing either vector (pGIPZ) or shRit2-107 were treated ±1μM PMA or ±20μM AIM-100, 10 min, 37°C, and both pY284Ack1 and total Ack1 levels were measured from parallel lysate aliquots by immunoblot. *Top*: Representative immunoblots. *Bottom*: Average pY284-Ack1 levels expressed as %vehicle-treated control cells ±SEM. ****p<0.0001, one-way with Dunnett's post-hoc comparison, n=6. **B**. *PKC-stimulated DAT-Rit2 dissociation*. HEK293T cells were triple-transfected with BBS-DAT, HA-Rit2, and either empty vector or S445P-Ack1-HA. Cells were treated ±1μM PMA, 30 min, 37°C, labeled with α-BTX-b, and DAT complexes were recovered by streptavidin pulldown as described in *Materials and Methods. Top*: Representative immunoblots. *Bottom*: Average DAT-Rit2 association expressed as %vehicle-treated control ±SEM. p=0.99, two-tailed Student's t test, n=4.